NR
91
4

DOT/FAA/NR-91/4

COPY 3

Gust Front/Wind Shift Detection Algorithm for the Terminal Doppler Weather Radar

Program Director
for Surveillance
Washington, D.C. 20591

FAA WJH Technical Center
00026693

National Severe Storms Laboratory
1313 Halley Circle
Norman, Oklahoma 73069

November 1989

MAY 26 1992
CENTER LIBRARY
ATLANTIC CITY, N.J. 08405

Final Report

This document is available to the public through the National Technical Information Service, Springfield, Virginia 22161.

U.S. Department of Transportation
Federal Aviation Administration

Notice

This document is disseminated under the sponsorship of the U.S. Department of Transportation in the interest of information exchange. The U.S. Government assumes no liability for the contents or use thereof.

Technical Report Documentation Page

1. Report No. DOT/FAA/NR-91/4	2. Government Accession No.	3. Recipient's Catalog No.
4. Title and Subtitle Gust Front/Wind Shift Detection Algorithm for the Terminal Doppler Weather Radar		5. Report Date November 1989
		6. Performing Organization Code MGG000
7. Author(s) Arthur Witt, Steven D. Smith, Michael D. Eilts Laurie G. Hermes, and Diana L. Kingle-Wilson		8. Performing Organization Report No.
9. Performing Organization Name and Address National Severe Storms Laboratory 1313 Halley Circle Norman, OK 73069		10. Work Unit No. (TRAIS)
		11. Contract or Grant No. DTFA01-80-Y-10524
12. Sponsoring Agency Name and Address US Department of Transportation Federal Aviation Administration 800 Independence Ave, SW Washington, DC		13. Type of Report and Period Covered Final Report
		14. Sponsoring Agency Code ANR-150

15. Supplementary Notes

16. Abstract

An algorithm for real-time detection of tornadoes, using single-Doppler radar data, is described. This algorithm searches for tornadic vortex signatures (TVS's) which are characterized by strong azimuthal shear in Doppler velocity fields. A TVS usually indicates that a tornado is occurring. The algorithm searches for azimuthal radial velocity differences, above a certain threshold, between adjacent gates at constant range. It then builds these "pattern vectors" into features for each scan in elevation, and finally determines the vertical correlation among features. When at least three features are vertically correlated and the lowest one is below a prescribed minimum-height threshold, a "TVS" is declared, indicating that a tornado is occurring. If the lowest feature is not below the height threshold, a "potential TVS (PTVS)" is declared, indicating that a tornado may soon occur.

The TVS algorithm has been tested on five tornadoes that occurred in Colorado and Missouri. Each tornado had an associated TVS, which was detected by the algorithm. In all cases, either a PTVS or TVS preceded each tornado, resulting in a 4 minute average lead time. Evaluated on a scan-by-scan basis, the Probability Of Detection (POD) is 78%. No TVS false alarms and only 3 PTVS false alarms occurred for these 5 cases. The algorithm was also tested on two rotating microbursts with no detections occurring.

17. Key Words Gust Front, Windspeed, Terminal Doppler, Doppler Radar Weather, Weather Radar, Weather Algorithm		18. Distribution Statement This document is available to the public through the National Technical Information Service, Springfield, VA 22161	
19. Security Classif. (of this report) Unclassified	20. Security Classif. (of this page) Unclassified	21. No. of Pages 76	22. Price

Form DOT F 1700.7 (8-72) Reproduction of completed page authorized

GUST FRONT/WIND SHIFT DETECTION ALGORITHM FOR THE TERMINAL DOPPLER WEATHER RADAR

Arthur Witt
Steven D. Smith
Michael D. Eilts

NOAA/Environmental Research Laboratories
National Severe Storms Laboratory
Norman, OK 73069

Laurie G. Hermes

Cooperative Institute for Mesoscale Meteorological Studies
University of Oklahoma
Norman, OK 73019

Diana L. Klingle-Wilson

Massachusetts Institute of Technology/Lincoln Laboratory
Lexington, MA 02173

PREFACE

We would like to thank Drs. Dusan Zrnić and Edward Brandes for valuable discussions and suggestions concerning this study. We also thank all those from MIT/Lincoln Laboratory and the National Severe Storms Laboratory who assisted in the collection of Doppler radar data. Joan Kimpel provided graphics support and the manuscript was typed by Carole Holder and Kelly Lynn.

Table of Contents

PREFACE i

LIST OF FIGURES iii

LIST OF TABLES v

ABSTRACT vi

1. INTRODUCTION 1

2. PATTERN RECOGNITION 3

3. FEATURE EXTRACTION 8

4. VERTICAL CONTINUITY 9

5. POLYNOMIAL CURVE FITTING 11

6. HORIZONTAL WIND ESTIMATION ON BOTH SIDES OF A DETECTED GUST FRONT 12

7. GUST FRONT TRACKING AND FORECASTING 17

8. PERFORMANCE ENHANCERS 17

9. TEST RESULTS 20

9.A. PROBABILITY OF DETECTION (POD) 23
9.B. FALSE ALARM RATIO (FAR) 34
9.C. PREDICTION EVALUATION 36
9.D. WIND ESTIMATE EVALUATION 44

10. SUMMARY AND CONCLUSIONS 54

11. REFERENCES 58

APPENDIX A 59

APPENDIX B 64

APPENDIX C 66

LIST OF FIGURES

Figure 1. Example of a pattern vector. Reflectivity factor Z (dBZ), radial velocity (m s^{-1}), and a nine-point average mean velocity are given. "B" and "E" denote the beginning and ending range of the pattern vector. "G" is the detected position of the front, i.e., the location of the peak shear. The location and length, in range, of each data window used by the wind shift algorithm is also shown (from Witt and Smith, 1987).

Figure 2. Criteria by which a pattern vector is saved (hatched area).

Figure 3. Geometry of the vertical continuity box. The uppercase "E's" denote the endpoints of the detected gust front and the lower case "c" denotes the centroid position. Initially determined size and location is dashed and the solid line box is its final location (from Witt and Smith, 1987).

Figure 4. Schematic showing detected gust front and the two data windows over which we estimate the horizontal wind. The adjustable parameters are: Δr is the range extent of the window; $\Delta\theta$ is the azimuthal extent of the window; and δr is the range offset of the window from the detected front (from Witt and Smith, 1987).

Figure 5. Example of an algorithm overlay plot.

Figure 6. Detections made on 4 September from 1957-2022 UT in 5 minute intervals for a gust front of strong to severe strength. The "+" represents the location of Stapleton Airport.

Figure 7. Detections made on 29 July from 2353-0029 UT in 4-5 minute intervals for a gust front of moderate strength.

Figure 8. POD, as a function of Percent Convergent Length Detected Threshold (% CLD_{min}), for moderate, strong, severe and all gust fronts.

Figure 9. POD, as a function of Percent Length Detected Threshold (% L_{min}), for moderate, strong, severe and all gust fronts (from Klingle-Wilson, et al., 1989).

Figure 10. Detections made on 16 March from 1955-2035 CST in 8-9 minute intervals for a gust front of strong to

severe strength. The "+" represents Will Rogers Airport.

Figure 11. Detections made on 24 May from 2356-0029 CST in 7-9 minute intervals for a gust front of strong to severe strength. The "+" represents Will Rogers Airport.

Figure 12. POD, as a function of Percent Convergent Length Detected Threshold (% CLD_{min}), for moderate, strong, severe and all gust fronts.

Figure 13. Histogram of time differences between 10-minute forecasts and actual positions. Negative (positive) values indicate a late (early) forecast.

Figure 14. Histogram of time differences between 20-minute forecasts and actual positions. Negative (positive) values indicate a late (early) forecast.

Figure 15. Time differences of 10-minute forecasts as a function of gust front strength. Category 1 gust fronts are weak, 2 are moderate, 3 are strong, and 4 are severe. The numbers beside the asterisks indicate the number of observations represented by the asterisk.

Figure 16. Time differences of 20-minute forecasts as a function of gust front strength. Category 1 gust fronts are weak, 2 are moderate, 3 are strong, and 4 are severe.

Figure 17. Location of mesonet stations, LLWAS sensors, Stapleton International Airport runways, and the FAA-Lincoln Laboratory FL-2 radar site.

Figure 18. Scatter plot of wind direction computed by the wind shift algorithm versus the average wind direction computed from mesonet data. The solid line represents a one-to-one correlation between the variables.

Figure 19. Difference between algorithm direction estimates and average wind directions computed from mesonet data.

Figure 20. Scatter plot of wind speeds computed by the wind shift algorithm versus averaged peak wind speed from mesonet data. The solid line represents a perfect correlation between the variables.

LIST OF TABLES

Table 1. POD and FAR statistics.

Table 2. Average Percent of Convergent Length Detected statistics.

Table 3. POD and FAR statistics.

Table 4. Average Percent of Convergent Length Detected statistics.

Table 5. POD and FAR statistics for 10- and 20-minute forecasts.

Table 6. Comparison of the forecast time of frontal passage with the actual time of frontal passage.

Table 7. Comparison of algorithm wind estimates with actual wind observations. (U) indicates uniform wind model; (P) indicates perpendicular wind model.

Table 8. Comparison of algorithm-generated and mesonet wind speeds.

ABSTRACT

During 1987, Doppler radar data were collected in Denver, Colorado and Norman, Oklahoma to test and evaluate the Gust Front Detection Algorithm, which is designed to detect the radial convergence associated with a gust front, forecast its future location, and estimate the wind speed and direction behind the front. This paper describes the version of the gust front algorithm which will be deployed in the initial Terminal Doppler Weather Radars. The algorithm uses two 360° low-elevation angle PPI's of radial velocity data. Radial convergence lines are detected and vertical continuity is used to associate detections and thus reduce false alarms. Recent enhancements to the algorithm include: 1) peak velocity difference thresholding, 2) variable thresholds for the two elevation scans, 3) connection of nearby shear features into a single shear feature, 4) a fifth-order polynomial fit to the radial convergence lines to allow more representative positioning of the gust front, 5) normal velocity component tracking and forecasting, 6) a velocity outlier rejection scheme, 7) redefinition of the data processing sector, 8) a perpendicular wind estimation technique for use with short gust fronts and as a replacement estimate when uniform wind model estimates fail error checks, and 9) rigorous error checking of wind estimates using gust front orientation and tracking information.

The performance evaluation of the algorithm was completed using the 1987 Colorado and Oklahoma data sets. The most notable results were the high PODs and the low FARs. Gust front forecasts were found to be, on average, within four minutes of the actual time of frontal passage. Wind estimates were generally within 30° and 3 m s^{-1} of the measured surface winds.

1. INTRODUCTION

A gust front is the region of rapid wind increase or shear at the leading edge of the cold air outflow from a thunderstorm. Wind shears and turbulence along the gust front are potentially hazardous to landing or departing aircraft. Because of this, the detection of gust fronts in the terminal environment is an integral part of the Federal Aviation Administration's (FAA) Terminal Doppler Weather Radar (TDWR) program.

The change of wind speed and direction in the terminal area associated with gust fronts and synoptic fronts also cause significant air traffic delays and excess fuel consumption due to time-costly runway configuration changes. During the Classify, Locate, and Avoid Wind Shear (CLAWS) project (McCarthy et al., 1986) it was determined that a 20-minute forecast of a wind shift at the airport was a useful product for air traffic management. This gives controllers time to redirect air traffic without significantly affecting airport operations.

The Gust Front/Wind Shift Detection Algorithm (hereafter called the Gust Front Algorithm) addresses both of these problems. When a wind shift is expected to affect airport operations within 20 minutes, a 10- and 20-minute forecasted location, as well as the expected wind vector behind the front is given to air traffic control so that plans for changing the approach and departure runways can be started, if necessary. When a gust front wind shift line is detected on or within three

miles of the end of the runway, wind shear warnings are generated.

The initial design and development of the Gust Front Algorithm was done by Uyeda and Zrnić (1985, 1986). This algorithm has the capability of detecting, within a field of Doppler radar velocities, the radial convergence lines which typically characterize a gust front. Limited testing by Uyeda and Zrnić showed that the algorithm could locate and track strong gust fronts that commonly occur in Oklahoma in the Spring. Additional testing of the algorithm prior to the 1987 TDWR experiment in Denver, CO revealed the need for further developmental work to allow the algorithm to detect weaker and smaller scale gust fronts. Major enhancements to the algorithm included the vertical association of gust front signatures at two low-altitude elevation scans to reduce false alarms, as well as a technique to supply horizontal wind estimates ahead and behind detected gust fronts. The report by Witt and Smith (1987) documented these enhancements and other refinements to the algorithm, such as proper threshold selection.

Another iteration of algorithm development followed field tests of the algorithm in the Denver area during 1987. Enhancements included a sophisticated velocity dealiasing scheme (Eilts and Smith, 1989), a technique to mitigate some ground clutter induced errors, better representation of the location of the gust front, and error checking of the wind estimates, along

with a perpendicular wind estimate as an alternative when uniform wind estimates are determined to be unreliable.

In this paper, we outline the principles of the gust front/wind shift algorithm that will be deployed initially in TDWR and discuss in-depth those aspects which have not been previously documented. The portion of the algorithm dealing with the detection of gust fronts is presented in Sections 2-5. Techniques for estimating the winds behind a gust front are given in Section 6. The procedure for tracking and forecasting gust fronts is presented in Section 7, and some recent specialized enhancements are given in Section 8. Test results using Doppler radar data collected during 1987 are presented in Section 9. There we present the Probability of Detection (POD) and False Alarm Ratio (FAR) (see Donaldson et al., (1975) for a definition of POD and FAR) for fourteen days when gust fronts were observed in the Doppler velocity data. Wind estimates generated by the algorithm are also compared to surface data to determine the reliability of the estimates. Appendix A gives a general outline of the algorithm and its various functions. Appendix B lists recommended values of some important adjustable parameters used in the Gust Front Algorithm and discussed in the text.

2. PATTERN RECOGNITION

The pattern recognition technique used in the Gust Front Algorithm is one which relies on identification of the main attribute which gust fronts possess in Doppler velocity fields,

i.e., lines of radial convergence. Detection of other attributes of gust fronts observed by Doppler radar, such as azimuthal shear and reflectivity thin lines, are not part of the present detection algorithm, but may be added in subsequent development. It is assumed that data artifacts such as ground clutter, second trip echoes, velocity aliases, and data in areas of low weather signal to receiver noise ratios are either corrected or removed prior to algorithm invocation.

The algorithm begins by computing a nine-point (seven point if the range gate spacing is greater than 200 m) running average to smooth the velocity data in range. Using the smoothed data, the algorithm searches along radials for shear segments (runs) of decreasing velocity (radial convergence). However, there is often substantial point-to-point variation of velocity in range. Therefore, when searching for segments, a seven-point (five if the range gate spacing is greater than 200 m) look ahead capability which allows for comparison of a particular valid velocity with the seven (five) adjacent velocities in range is used. The algorithm accepts the velocity within the group of seven (five) which is closest to, but less than or equal to, the velocity in question. If radial convergence is detected, the next iteration compares the chosen velocity with the next seven (five) values in range. If there is an increase in radial velocity over seven (five) consecutive points in range, a segment terminates.

The main attributes of a segment are consolidated into a seven component pattern vector. Each pattern vector consists of: 1) azimuth angle, 2) beginning slant range, 3) ending slant range, 4) beginning radial velocity, 5) ending radial velocity, 6) peak or maximum radial shear over a distance of ~1 km within the shear segment, and 7) slant range to the location of the peak shear. Figure 1 shows an example of a pattern vector.

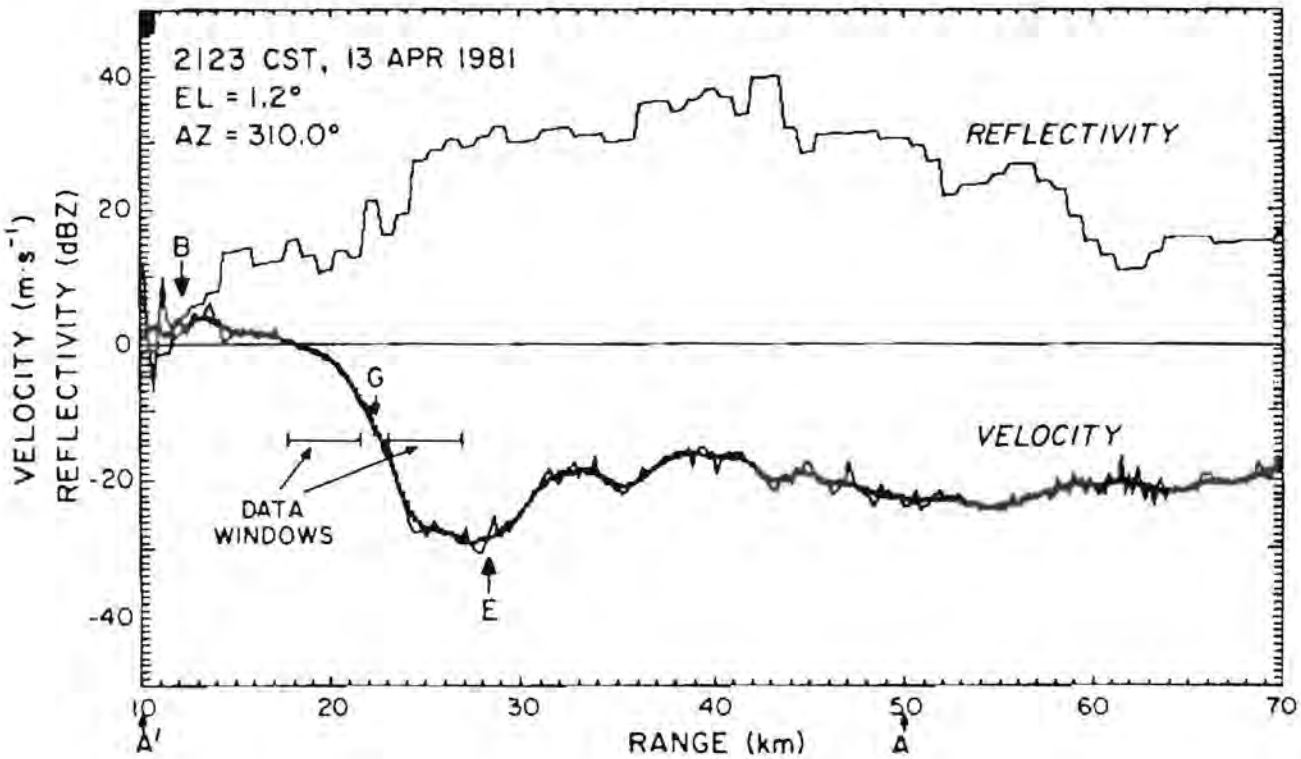

Figure 1. Example of a pattern vector. Reflectivity factor Z (dBZ), radial velocity (m s^{-1}), and a nine-point average mean velocity are given. "B" and "E" denote the beginning and ending range of the pattern vector. "G" is the detected position of the front, i.e., the location of the peak shear. The location and length, in range, of each data window used by the wind shift algorithm is also shown (from Witt and Smith, 1987).

The peak radial shear and differences between the beginning and ending velocity, ΔV, are compared to minimum thresholds to determine whether a pattern vector is saved. This differs from the procedure described by Uyeda and Zrnić (1986) who used two shear thresholds and a minimum and maximum "flux" threshold. Test results have also shown that when the peak or maximum velocity difference, over a distance of ~1 km (eight or six range gates) within the shear segment, is greater than the beginning to ending velocity difference, the shear segment is usually associated with ground clutter or noisy data. Therefore, a pattern vector whose peak velocity difference is greater than its beginning to ending velocity difference is discarded.

The algorithm operates on two low-level scans with different elevation angles (~0.5°, 1.0°), but thresholds for ΔV are different for each scan. The appropriate threshold values are determined by the minimum strength of gust fronts which need to be detected. Gust front strength is based on the average ΔV over its azimuthal extent. The strength categories are given as follows: weak, ΔV = 5-10 m s^{-1}; moderate, ΔV = 10-15 m s^{-1}; strong, ΔV = 15-25 m s^{-1}; and severe, ΔV > 25 m s^{-1}. Because it is desirable to detect all moderate and stronger gust fronts, the current minimum ΔV threshold for saving pattern vectors is set at 7 m s^{-1} for the lowest scan level. This threshold is relaxed slightly for the upper of the two tilts (elevation angles) with the minimum ΔV set at 5 m s^{-1}, because contamination by ground

clutter residue at the higher tilt is less likely. These appear to work well for detecting gust fronts of moderate or greater strength in the Denver, CO area. The peak shear threshold is the same at both scans, 2 m s^{-1} km^{-1}. Figure 2 shows the criteria by which a pattern vector is saved for the upper tilt.

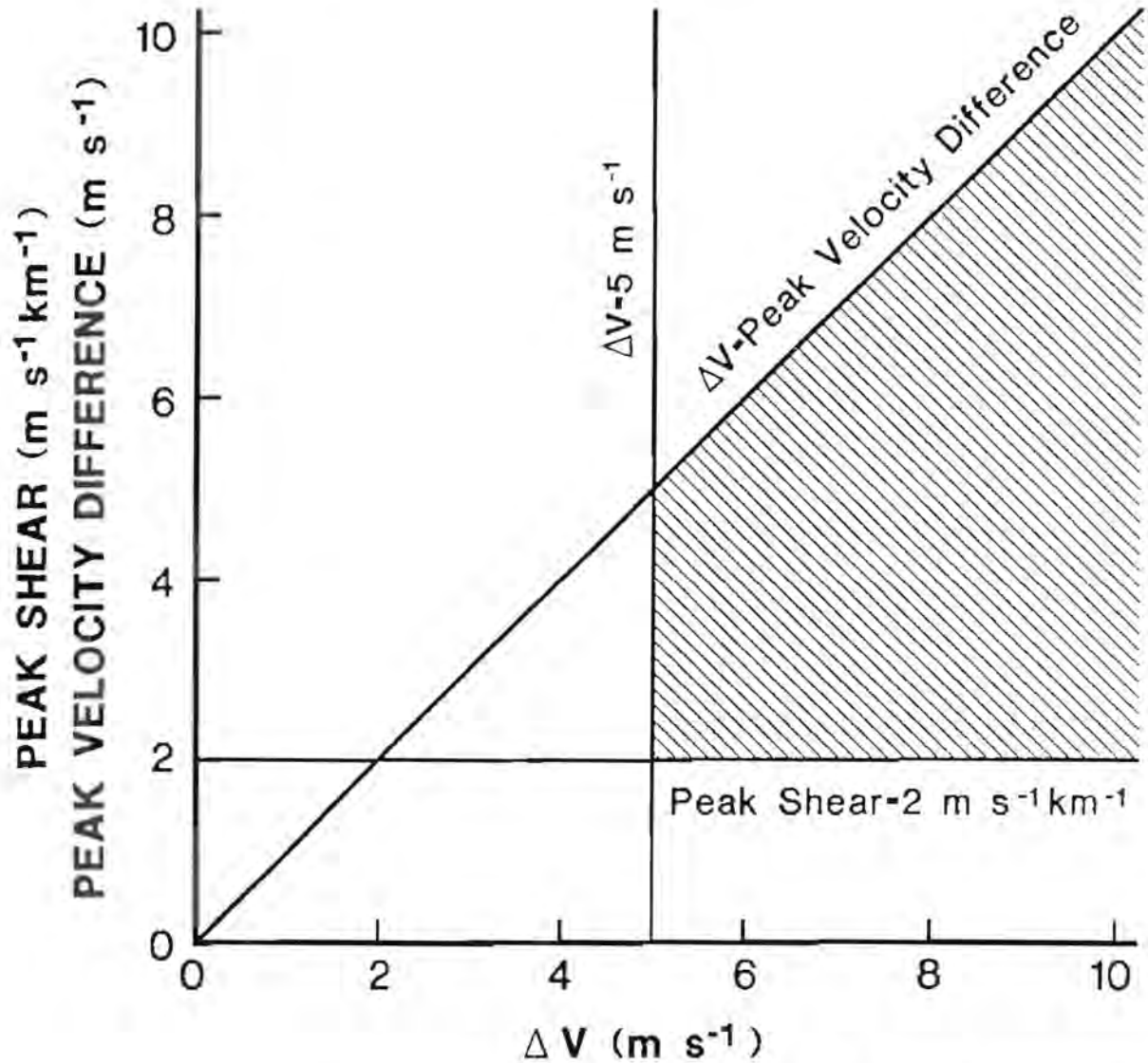

Figure 2. Criteria by which a pattern vector is saved (hatched area).

3. FEATURE EXTRACTION

Individual pattern vectors are combined into features based on spatial proximity. (Features are groups of pattern vectors which may later be combined into gust fronts). Witt and Smith (1987) sort pattern vectors into a common feature if they are separated in azimuth by no more than 2.2° and if the locations of the peak shears are within 2 km in range. If, after sorting, there are fewer than five vectors in any one feature, that feature is discarded. Furthermore, if the length of the feature (defined as the distance between end points of the feature) is not at least 5 km, that feature is also discarded. The minimum number of pattern vectors per feature (5) and the length threshold (5 km), are those recommended by Witt and Smith (1987) for the Denver environment.

After pattern vectors are sorted into features, those features in close proximity to other features are combined. Two features are combined if the endpoints of the features are within some specified distance. For the Denver environment, a 5 km search radius works well.

Combining pattern vectors into features and feature connecting are performed for each of the two low-level scans. The next step is to use vertical continuity to associate detections among the two scans.

4. VERTICAL CONTINUITY

In order to reduce the number of false alarms, potential gust front features are subjected to a vertical continuity check using data from two low-level scans (~0.5, 1.0°). For two features detected at different elevation scans to satisfy the vertical continuity requirement, it is necessary for the centroid of one feature to be within the "vertical continuity box" of the other feature. The centroid is determined by averaging the locations of all pattern vectors in the feature. The "vertical continuity box" of a feature is described by a rectangle which is obtained by drawing lines 5 km either side of a line connecting the endpoints of the feature and then shifting the box until its centroid is aligned with the centroid of the feature (Fig. 3). Vertical continuity boxes are generated for features at both elevation scans. Thus, vertical continuity can be established either by having the centroid of a feature at the upper tilt fall within the box of a feature at the lower tilt, or by having the centroid of a feature at the lower tilt fall within the box of a feature at the upper tilt. Testing showed a large reduction in the FAR after vertical continuity checks were added to the algorithm (Witt and Smith, 1987).

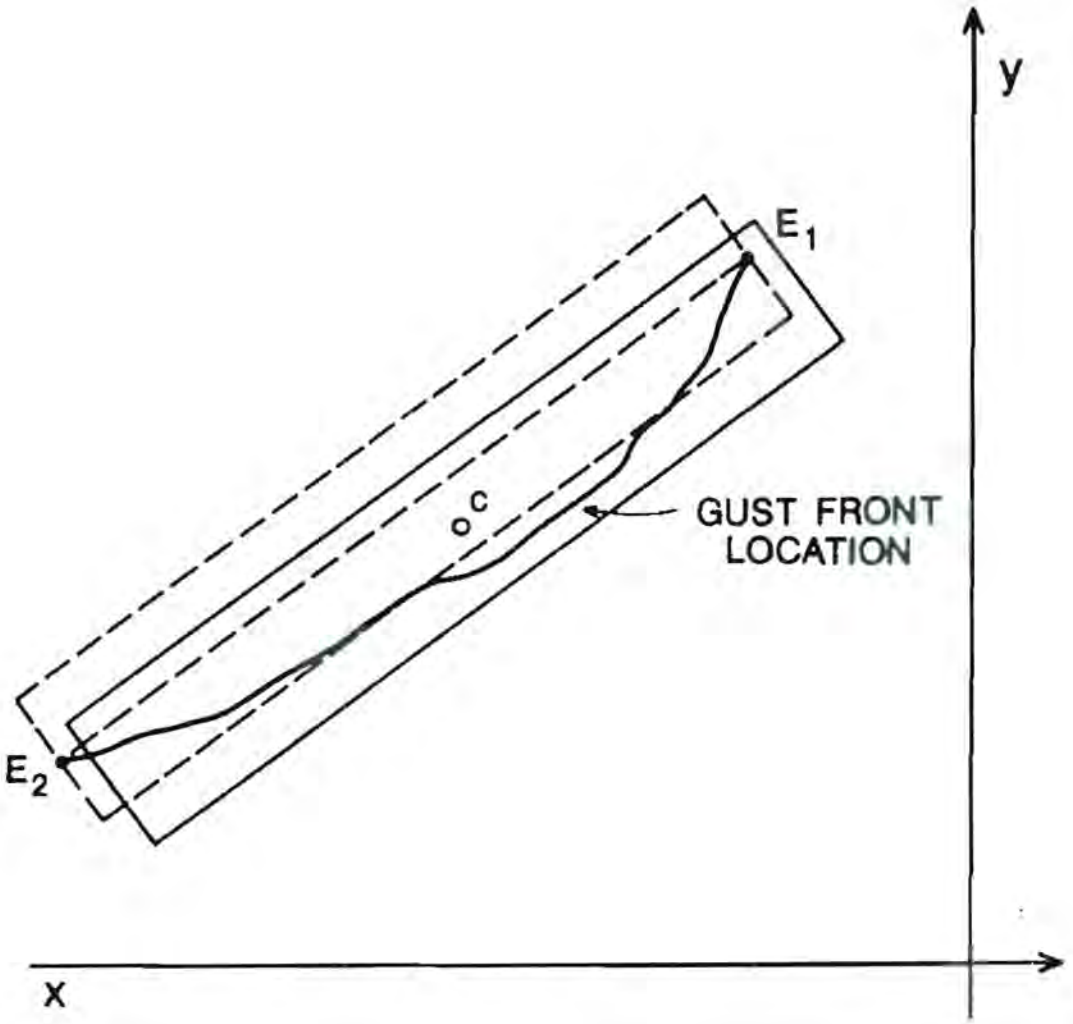

Figure 3. Geometry of the vertical continuity box. The uppercase "E's" denote the endpoints of the detected gust front and the lower case "c" denotes the centroid position. Initially determined size and location is dashed and the solid line box is its final location (from Witt and Smith, 1987).

5. POLYNOMIAL CURVE FITTING

In the original version of the Gust Front Algorithm, a second-order polynomial in range and azimuth was fit to the points of peak shear of a detected feature (Uyeda and Zrnić, 1986) using the method of least-squares. More recently, the polynomial fitting was performed in Cartesian coordinates to better accommodate gust front tracking (Witt and Smith, 1987). The curve fitting occurred prior to feature connecting and vertical continuity checks. When algorithm output was graphically displayed, the gust fronts were plotted as a series of features connected by line segments. Sometimes this resulted in unrealistic "kinks" in the displayed results.

For aesthetic reasons, it was decided that polynomial curve fitting in Cartesian coordinates be performed after the vertical continuity check. A fifth-order polynomial

$$y = b_0 + b_1x + b_2x^2 + b_3x^3 + b_4x^4 + b_5x^5 \qquad (1)$$

is used to describe the gust front location if the front's length is greater than 20 km. For lengths ≤ 20 km, a third-order polynomial describes the gust front location. The subscripted constants in (1) are the polynomial coefficients and (x,y) are Cartesian coordinate pairs defined in a local coordinate system such that the line connecting the ends of the gust front is parallel to the x-axis and the y-axis passes through the centroid. Once the front has been described by the appropriate

polynomial, the front's length is calculated as the path length from end point to end point.

A recent addition to curve fitting combines features from both low-level scans to be used in estimating the polynomial coefficients. The displayed results are now smoother and appear to not overly distort the true locations of the peak shear.

6. HORIZONTAL WIND ESTIMATION ON BOTH SIDES OF A DETECTED GUST FRONT

Incorporated as part of the Gust Front Algorithm is a technique to estimate the horizontal wind ahead and behind the gust front using a least-squares technique (Witt and Smith, 1987). This technique is very similar to that used by the Next Generation Weather Radar (NEXRAD) Sectorized Uniform Wind algorithm (Smith, 1986). Initial testing of this portion of the algorithm began during the 1987 TDWR experiment in Denver.

Using data from the lower elevation angle tilt, the wind estimation portion of the algorithm relies on the assumption of a uniform, horizontal wind within specified spatial sectors (uniform wind model). For each detected gust front, sectors are offset by δr in range from the front (~2 km) and extend in range by an amount Δr (~2.5 km). The azimuthal width of the sectors is $\Delta\theta$ (>30°) (Fig. 4). The parameters Δr, δr, and $\Delta\theta$ are user selectable. Recommended settings for these parameters are given in Appendix C.

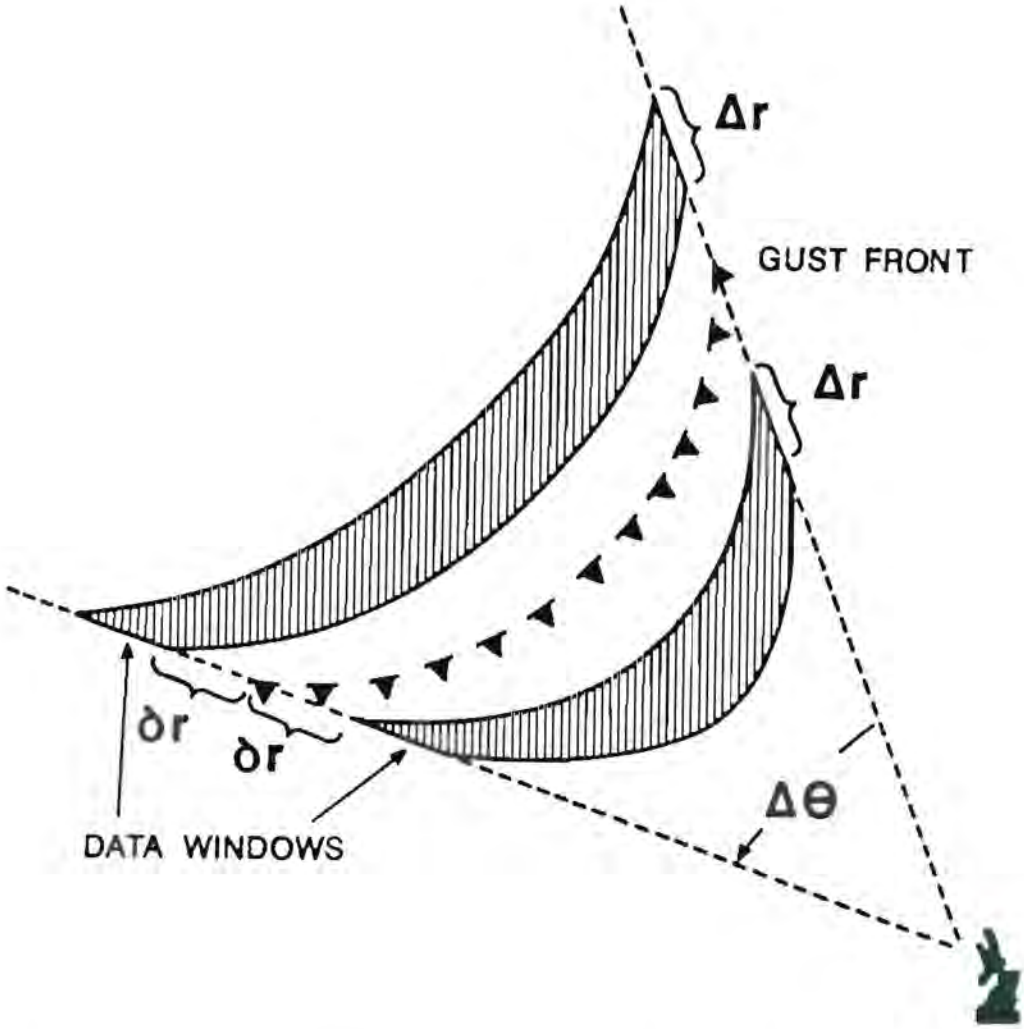

Figure 4. Schematic showing detected gust front and the two data windows over which we estimate the horizontal wind. The adjustable parameters are: Δr is the range extent of the window; $\Delta\theta$ is the azimuthal extent of the window; and δr is the range offset of the window from the detected front (from Witt and Smith, 1987).

The relationship between the radial velocity, v_r, and the wind components (u_o, v_o) for a uniform, horizontal wind is

$$v_r = u_0 \sin\theta \cos\phi + v_0 \cos\theta \cos\phi + \varepsilon \qquad (2)$$

where u_o is positive eastward, v_o is positive northward, θ is azimuth angle from north, ϕ is radar elevation angle, and ε is a small but unknown error owing to Doppler velocity measurement uncertainty.

For low elevation angles ($\phi < 2°$), $\cos\phi \sim 1$, so the elevation dependence can be neglected in (2) without serious consequences. Estimates of the wind components, $(\hat{u}_o, \hat{v}_o)$, are obtained from regressing the smoothed Doppler velocities within each data sector onto the functions $\sin\theta$ and $\cos\theta$, and minimizing the sum of the squared errors, ε^2. Details of the linear regression can be found in Smith (1986).

There is uncertainty in $(\hat{u}_o, \hat{v}_o)$ owing to Doppler velocity measurement uncertainty. This estimate uncertainty increases as the sector's azimuthal width, $\Delta\theta$, decreases. Thus, a lower limit on the sector width of 30° is used. At this value, the uncertainty in the wind estimates nearly equals that of the individual Doppler velocity measurements. Smith and Rabin (1989) provide a detailed error analysis of the approach described in this section.

The azimuthal extent of many gust fronts is, however, smaller than 30°. For these gust fronts, where large estimation errors in $\hat{u}_o$ and $\hat{v}_o$ are possible, or when uniform wind estimates for longer gust fronts are not reasonable, the horizontal wind direction behind the front is assumed to be perpendicular to the gust front orientation angle (perpendicular wind model). The

orientation angle is the angle from east subtended by the straight line connecting the end points of the detected gust front. For outflow perpendicular to the gust front orientation, the Doppler velocity, v_r, and the horizontal wind speed, $|V|$, are related by

$$v_r = |V| \cos\psi + \varepsilon \tag{3a}$$

where the angle ψ is the difference between the radar azimuth and the angle perpendicular to the gust front orientation. Using linear regression techniques, the estimate of the wind speed behind the gust front, $|\dot{V}|$, is given by

$$|\dot{V}| = \frac{\sum_{i}^{N} v_{ri} \cos\psi_i}{\sum_{i}^{N} \cos^2\psi_i} \tag{3b}$$

with the summations over all N data points within the specified spatial sector. Hence, the wind speed estimate is a weighted average, in a least-squares sense, of the wind component perpendicular to the front.

A recent enhancement to the wind estimation portion of the algorithm is an outlier rejection scheme. After an initial least-squares fit of the radial velocity data, points are rejected if they are not within two root mean square errors (RMSE) about the fit. The RMSE is the square root of the mean of

the squared differences between data points and their fitted values. After removing outliers, a second fit of the data is performed. This two-pass fit is designed to reject anomalous data which can sacrifice the integrity of the horizontal wind estimates. The RMSE values, after outlier rejection, are used to determine wind estimate quality. From experience, if, after the second fit, values of the RMSE are larger than 3 m s^{-1}, the wind estimates are usually unreliable.

After time continuity has been established for a gust front, tracking and orientation information are used to determine the outflow side and also to error check the horizontal wind estimates behind the front. On occasion, significant nonuniformities in the wind field behind longer gust fronts can occur. As a result, wind estimates with directions that are quasi-parallel to the gust front orientation may be produced. Such wind estimates are rejected if their directions are less than 25° (variable threshold) different than the orientation of the gust front (i.e., nearly parallel to the gust front). Wind direction estimates for both long and short gust fronts are also checked against gust front propagation direction. Estimates with a component opposite the propagation direction are rejected. Wind estimates with extreme magnitudes (> 40 m s^{-1} for Denver) are also rejected by the algorithm. Wind estimates for the longer gust fronts that fail these error checks are replaced with the perpendicular wind model estimate.

7. GUST FRONT TRACKING AND FORECASTING

If one or more gust fronts are detected on two consecutive radar volume scans, an attempt is made to establish time continuity between the gust fronts. If the distance between the two gust front centroids is less than a distance threshold (equal to the distance a gust front moving at 33.3 ms^{-1} would cover in the time between consecutive radar scans), then time association is established. If there is more than one association in time, the algorithm chooses the front whose centroid is the closest.

The original version of the algorithm used a simple centroid to centroid method for determining the propagation vector for use in tracking and forecasting the future positions of gust fronts. Initial testing of this method showed that large errors were common, with fronts at times being forecast to move long distances almost parallel to their orientation. In order to alleviate this problem, the propagation vector is now calculated by using the component of the centroid to centroid vector which is perpendicular to the line connecting the endpoints of the gust front. This was found to work much better than the previous method.

8. PERFORMANCE ENHANCERS

Data artifacts, such as velocity aliases and ground clutter contaminated velocities, were found to adversely affect algorithm performance. The wind estimation technique suffers the most from these data artifacts. Also, false detections by the Gust Front

Algorithm often occur near large regions of ground clutter. Two major enhancements were added to the algorithm to improve performance: 1) a local environment dealiasing scheme (Eilts and Smith, 1989), and 2) clutter suppression windows.

The local environment dealiasing scheme was designed to automatically edit and dealias Doppler radial velocity data in real-time. Editing and dealiasing is accomplished by a series of comparisons of a velocity in question with neighboring values, both along the same radial and in an adjacent radial. Within this two-dimensional approach, there are a number of error checks designed to prevent errors from occurring or if they do, prevent them from propagating. This procedure has been found to perform much better than one-dimensional techniques which utilize only single radials. A description of this dealiasing technique can be found in Eilts and Smith (1989).

Spatial variations in ground clutter can introduce spurious radial gradients of Doppler velocity, resulting in the generation of pattern vectors and sometimes gust front features. Ground clutter cancelers reduce clutter problems to some extent but not entirely, and clutter residue maps identify regions where filtering is not sufficient. If both of these fail to prevent false detections, a user selectable clutter suppression window can be activated. The idea behind clutter suppression windows is to eliminate features which are located in regions of known ground clutter contamination. For example, in the Denver, CO. area, the mountains are a preferred region for false detections.

By specifying a clutter suppression window, features whose centroids lie within these windows are discarded. Preliminary results show that most false alarms can be eliminated in this manner.

In addition to the above two major enhancements, others include:

1) If the longest feature in the volume scan is above a specified length threshold (presently 15 km), but does not have vertical continuity, it is declared a detected front. This allows for the detection of long, but shallow gust fronts at distant ranges.

2) Due to ground clutter contamination and beam blockage, it is often difficult to detect a gust front within 10 km of the radar at the lower of the two tilts. Therefore, if no fronts are detected within 10 km of the radar, but a feature longer than the minimum front length threshold is detected at the upper tilt within 10 km of the radar, it is added to the list of detected fronts. This enhancement should only be used if the radar has a ground clutter filter. Otherwise, many false detections may occur.

3) Regardless of how strong and well defined a gust front is in the Doppler velocity field, the algorithm will not be able to detect it as it gets closer to and eventually passes over the radar site. In order to continue tracking detected gust fronts as they pass over the radar, a technique for "overhead tracking" is used, and operates as follows. If a gust front is detected

within 10 km of the radar and has a propagation speed of at least 4 m s^{-1} , its location and propagation vector are saved for possible overhead tracking. On the next volume scan, the centroid of the saved front is translated by its propagation velocity and a check is made to see if any detections were made near the new centroid location. If a detection is made near the centroid location, or if the centroid has translated beyond 10 km from the radar, the process is aborted. If the process is aborted because of a new detection within 10 km of the radar, it is restarted using the new detection, provided that its propagation speed is at least 4 m s^{-1}. If the process is not aborted, then the old location of the front is translated by its propagation vector and plotted. This process of translation and plotting continues until the front is once again detected on the other side of the radar, or until the centroid moves beyond 10 km of the radar.

9. TEST RESULTS

The latest version of the Gust Front Algorithm was tested on data collected during 1987 in both Colorado and Oklahoma. The Colorado data was collected by the FAA - Lincoln Laboratory FL-2 Doppler radar at Denver, and the Oklahoma data by the National Severe Storms Laboratory (NSSL) at Norman.

Evaluation of the radial convergence detection capability of the algorithm was done by running the algorithm on a volume scan of data, generating an algorithm overlay plot (as shown in

Fig. 5), and placing this overlay plot on top of a color display of the single Doppler velocity field for the 0.5° tilt. Since the algorithm only detects radial convergence, only the convergent parts of gust fronts were used to evaluate its

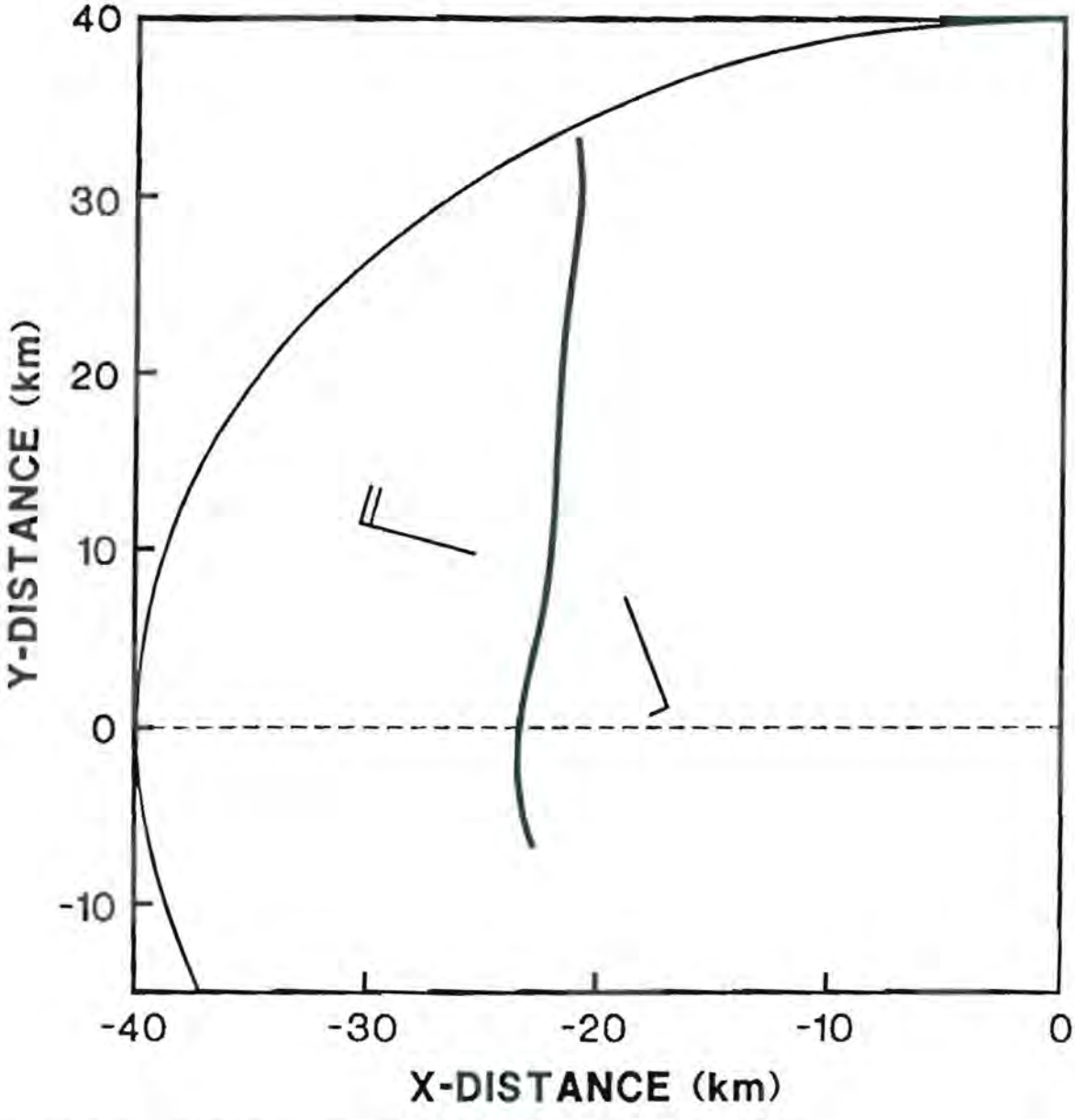

Figure 5. Example of an algorithm overlay plot.

detection capability - azimuthal shear, reflectivity thin lines, and/or strong flow against missing data were not considered. However, further testing on 1988 radar data did evaluate the algorithm based on radial convergence, azimuthal shear, and reflectivity thin line data. The results will be shown below. Also very weak, small, and/or short lived gust fronts were not used. At a minimum, a gust front had to have a radial velocity difference (ΔV) of at least 5 m s^{-1} over a length of at least 10 km along the gust front and persist for at least 10 minutes. The strength of a gust front was determined subjectively from the color displays of the radial velocity field. Gust front strengths were defined as

Weak: $\Delta V = 5\text{-}10$ m s^{-1}

Moderate: $\Delta V = 10\text{-}15$ m s^{-1}

Strong: $\Delta V = 15\text{-}25$ m s^{-1}

Severe: $\Delta V > 25$ m s^{-1}.

The prediction capability of the algorithm was also evaluated, but in slightly different ways for the Colorado and Oklahoma data. For the Colorado data, the predicted location of the gust front for both 10- and 20-minute forecasts was compared with the true gust front location at the valid time of the forecast. For the Oklahoma data, the predicted time of gust front passage over Will Rogers Airport in Oklahoma city was compared with the actual reported time of frontal passage.

Ground truth for the evaluation of algorithm-generated wind estimates is derived from a set of mesonet stations for the Colorado data, and from the National Weather Service (NWS) surface wind observations at Oklahoma City (OKC) for the Oklahoma data. Since winds ahead of a gust front are measured at the airport (via the Low-Level Wind Shear Alert System (LLWAS)) the emphasis of the evaluation will be restricted to wind estimates behind the front. The evaluation will determine how the algorithm estimates are related to the surface wind observations and the error bounds of the algorithm estimates.

9.A. PROBABILITY OF DETECTION (POD)

1) COLORADO DATA

Eleven days were chosen from the 1987 TDWR Denver Experiment for scoring algorithm performance. During these 11 days, 73 gust fronts of various strengths occurred, and at least one gust front per day reached moderate or greater strength. Examples of algorithm detections made on two days (4 September and 29 July) are shown in Figures 6 and 7.

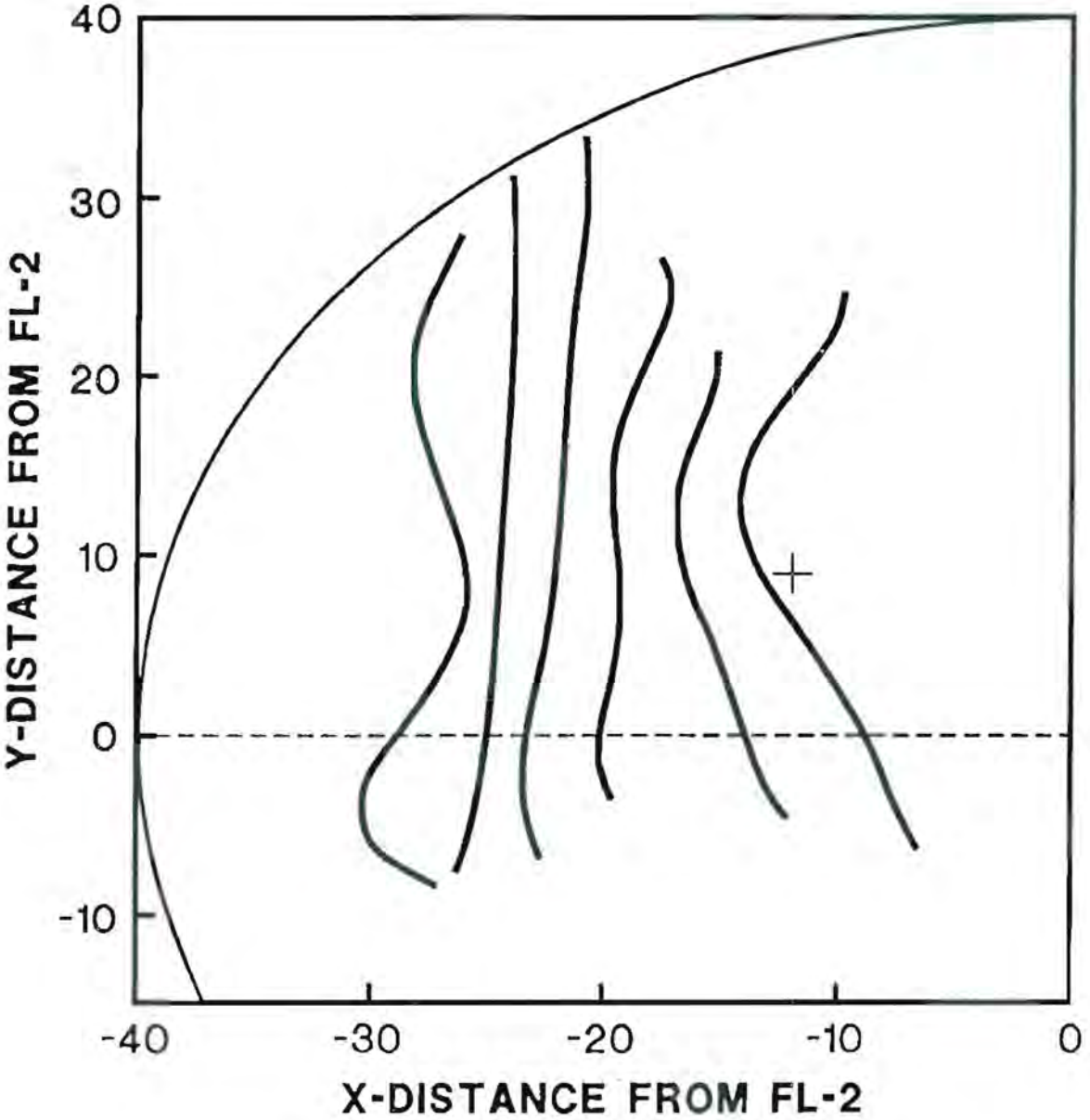

Figure 6. Detections made on 4 September from 1957-2022 UT in 5 minute intervals for a gust front of strong to severe strength. The "+" represents the location of Stapleton Airport.

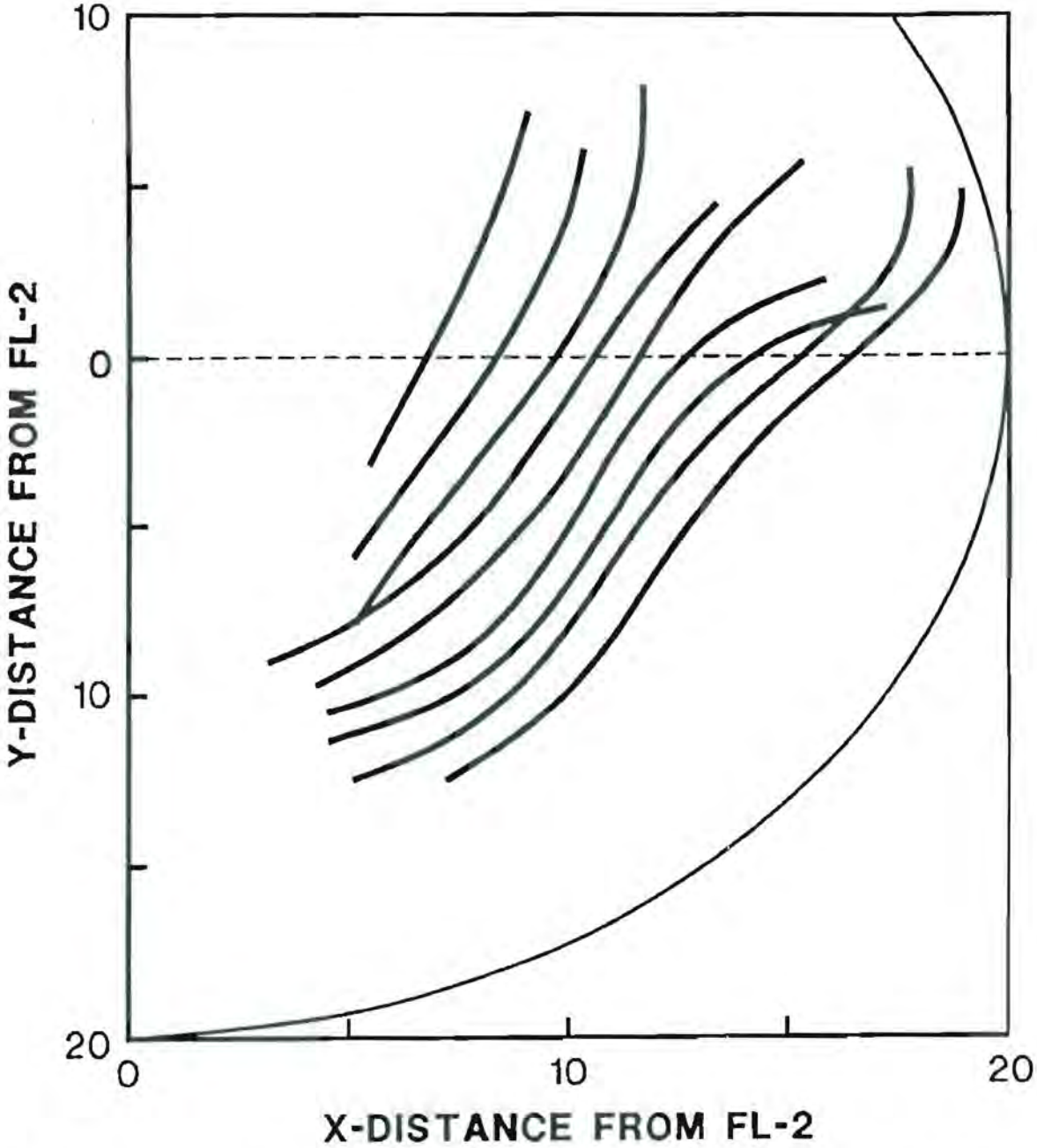

Figure 7. Detections made on 29 July from 2353-0029 UT in 4-5 minute intervals for a gust front of moderate strength.

Table 1 summarizes the probability of detecting any part of a gust front that occurred within 60 km of the radar. Due to the minimal operational impact expected from weak gust fronts, PODs were only calculated for gust fronts of moderate strength or

greater. The individual daily PODs varied from a low of 68% to a high of 100%. The overall probability of detecting any part of a moderate, strong, or severe gust front was 79%, 92%, and 100% respectively. The above POD's, however, do not indicate how well a gust front is actually detected. A few of the detections in Table 1 accounted for 50% or less of the convergent length of the gust front. Therefore, it is useful to apply a minimum Percent of Convergent Length Detected (%CLD) threshold ($\%CLD_{min}$), such that %CLD must exceed the threshold before a valid detection is declared. POD, as a function of $\%CLD_{min}$, is plotted in Figure 8. The average Percent of Convergent Length Detected, as a function of gust front strength, is given in Table 2.

Further testing, using 1988 radar data, was done to evaluate the detection capability of the algorithm based on radial convergence, azimuthal shear, and reflectivity thin line data, (i.e., the total gust front) and is discussed in detail in Klingle-Wilson et al., (1989). Here we present their plot of POD as a function of minimum Percent of Length Detected threshold (Fig. 9). In this case, the total length of the gust front, as indicated by radial convergence, azimuthal shear, and/or reflectivity this line data is used, versus just radial convergence for Fig. 8. As expected, the POD curves are lower for Fig. 9 versus Fig. 8, since the algorithm is presently not capable of detecting the portions of a gust front having azimuthal shear and/or a reflectivity thin line. Inclusion of

techniques to detect reflectivity thin lines and azimuthal shear are planned as future improvements to the algorithm.

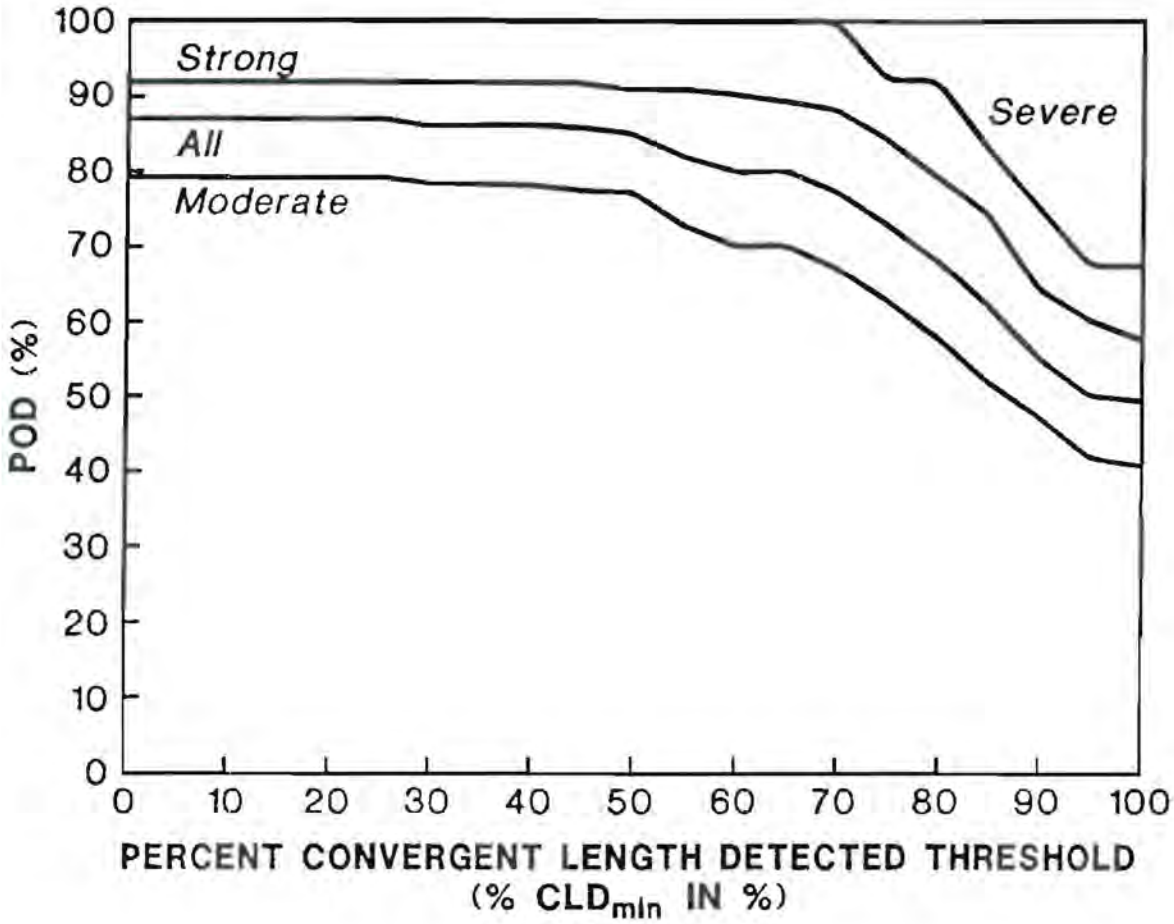

Figure 8. POD, as a function of Percent Convergent Length Detected Threshold (%CLD_{min}), for moderate, strong, severe and all gust fronts.

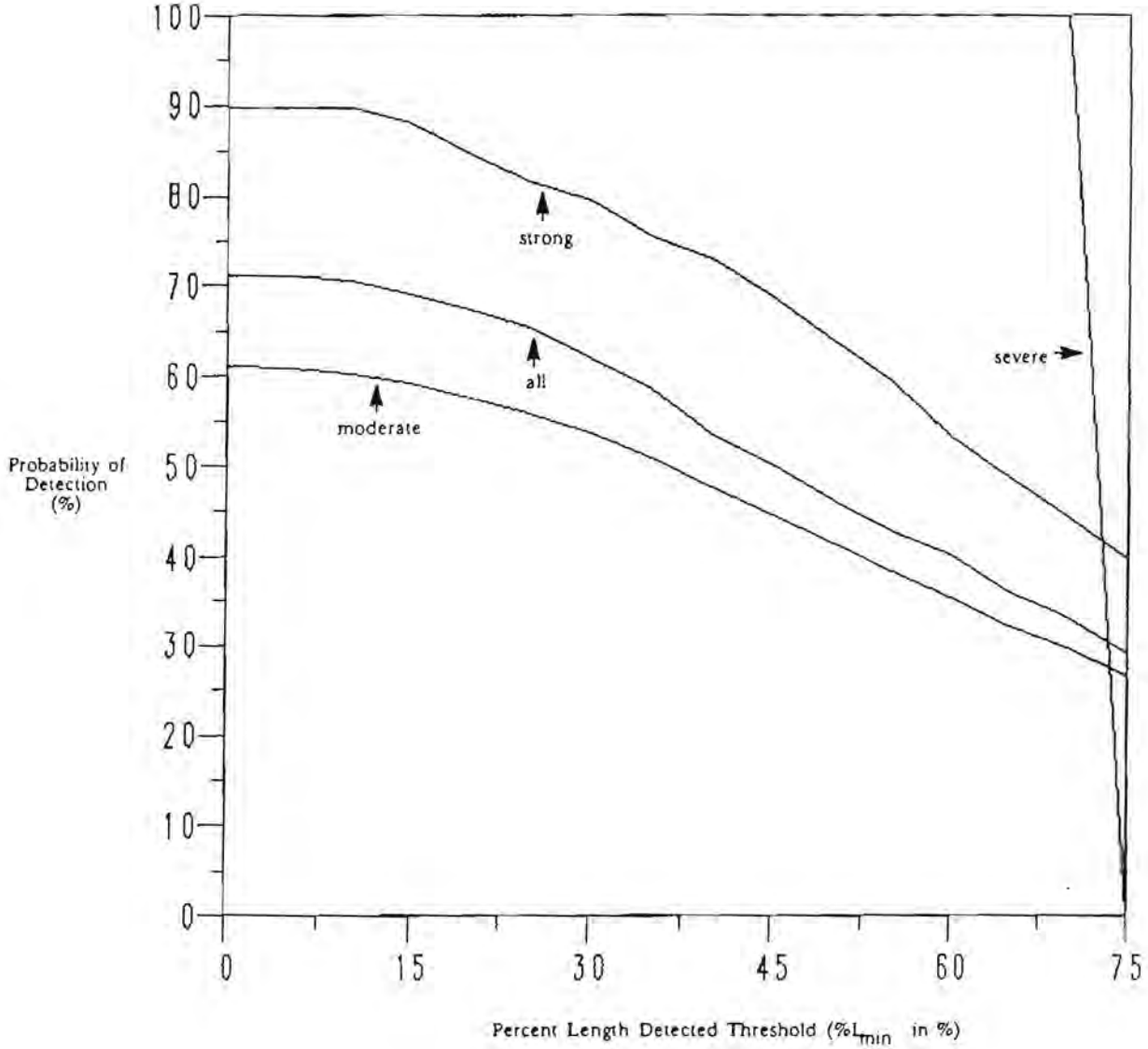

Figure 9. POD, as a function of Percent Length Detected Threshold ($\%_{min}$), for moderate, strong, severe and all gust fronts (from Klingle-Wilson, et al., 1989).

Table 1. POD and FAR statistics.

GUST FRONT ALGORITHM TEST RESULTS FROM 1987 TDWR DATA

Date	Probability of Detecting any part of the gust front Moderate	Strong	Severe	Total true detections	False alarms	FAR(%)
6/10	13/19 68%	-	-	17	0	0
6/14	7/7 100%	10/14 71%	-	19	0	0
6/18	14/19 74%	24/27 89%	9/9 100%	59	3	5
7/28	45/57 79%	8/8 100%	-	81	5	6
7/29	16/19 84%	7/7 100%	-	26	0	0
7/30	4/5 80%	-	-	4	0	0
7/31	28/38 74%	8/8 100%	2/2 100%	56	3	5
8/25	8/8 100%	6/6 100%	-	24	0	0
8/28	7/10 70%	-	-	12	0	0
9/02	6/7 86%	6/6 100%	-	16	0	0
9/04	12/14 86%	14/14 100%	1/1 100%	33	0	0
Totals	160/203 79%	83/90 92%	12/12 100%	347	11	3%

Table 2. Average Percent of Convergent Length Detected Statistics.

GUST FRONT ALGORITHM TEST RESULTS FROM 1987 TDWR DATA

Date	Average % of Convergent Length Detected Moderate	Strong	Severe	Total	Volume scans analyzed
6/10	75	-	-	75	29
6/14	91	83	-	86	13
6/18	90	98	97	95	48
7/28	87	91	-	88	59
7/29	90	100	-	93	29
7/30	73	-	-	73	10
7/31	94	76	83	90	29
8/25	75	95	-	84	20
8/28	89	-	-	89	48
9/02	81	96	-	89	38
9/04	86	93	90	90	30
Totals	87%	92%	94%	89%	353

2) OKLAHOMA DATA

In addition to the rather extensive testing done using Colorado data, a small subset of data collected during the 1987 DOPLIGHT Experiment (Forsyth et al., 1989) was also analyzed to further score the algorithm's performance, especially on stronger gust fronts. Each of the three days studied had a severe gust front which passed over OKC. Examples of algorithm detections made on 16 March and 24 May are shown in Figures 10 and 11.

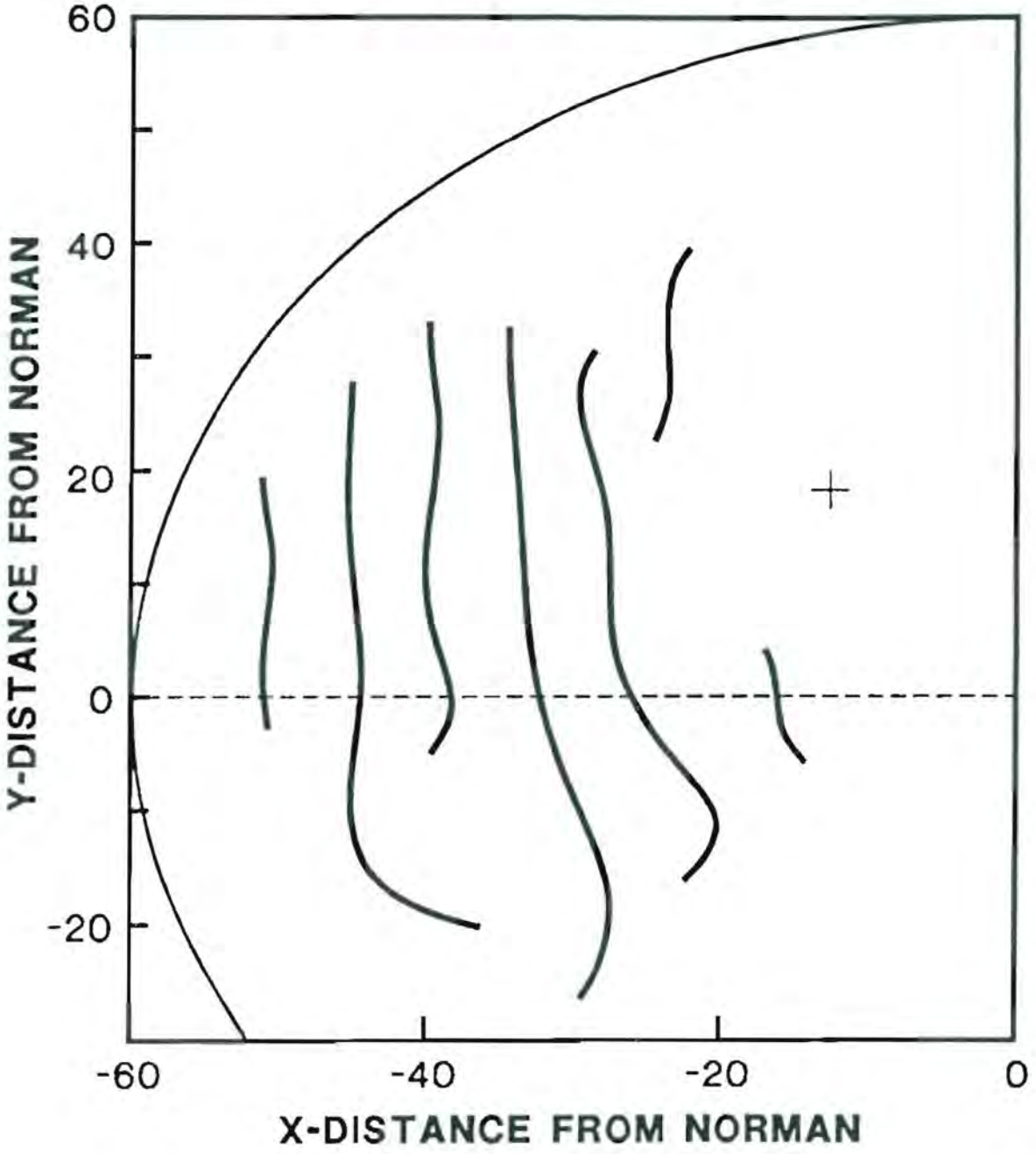

Figure 10. Detections made on 16 March from 1955-2039 CST in 8-9 minute intervals for a gust front of strong to severe strength. The "+" represents Will Rogers Airport.

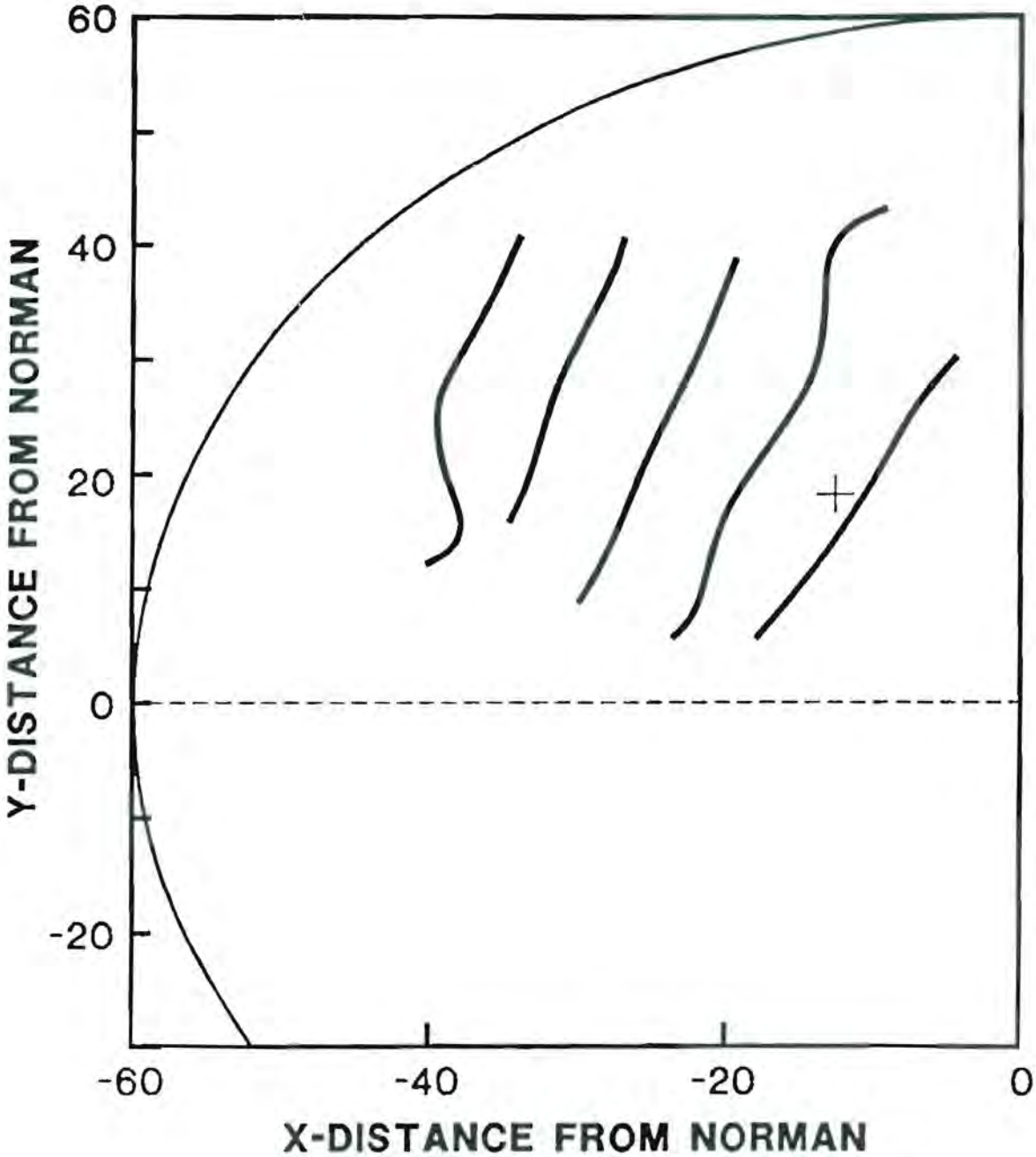

Figure 11. Detections made on 24 May from 2356-0029 CST in 7-9 minute intervals for a gust front of strong to severe strength. The "+" represents Will Rogers Airport.

Table 3 summarizes the probability of detecting any part of the gust front that occurred within 60 km of the radar. The algorithm was run using the same thresholds used on the Colorado data. The overall PODs were 71% for moderate, and 100% for both strong and severe gust fronts. POD as a function of % CLD_{min} is plotted in Fig. 12 and the average Percent of Convergent Length Detected is given in Table 4.

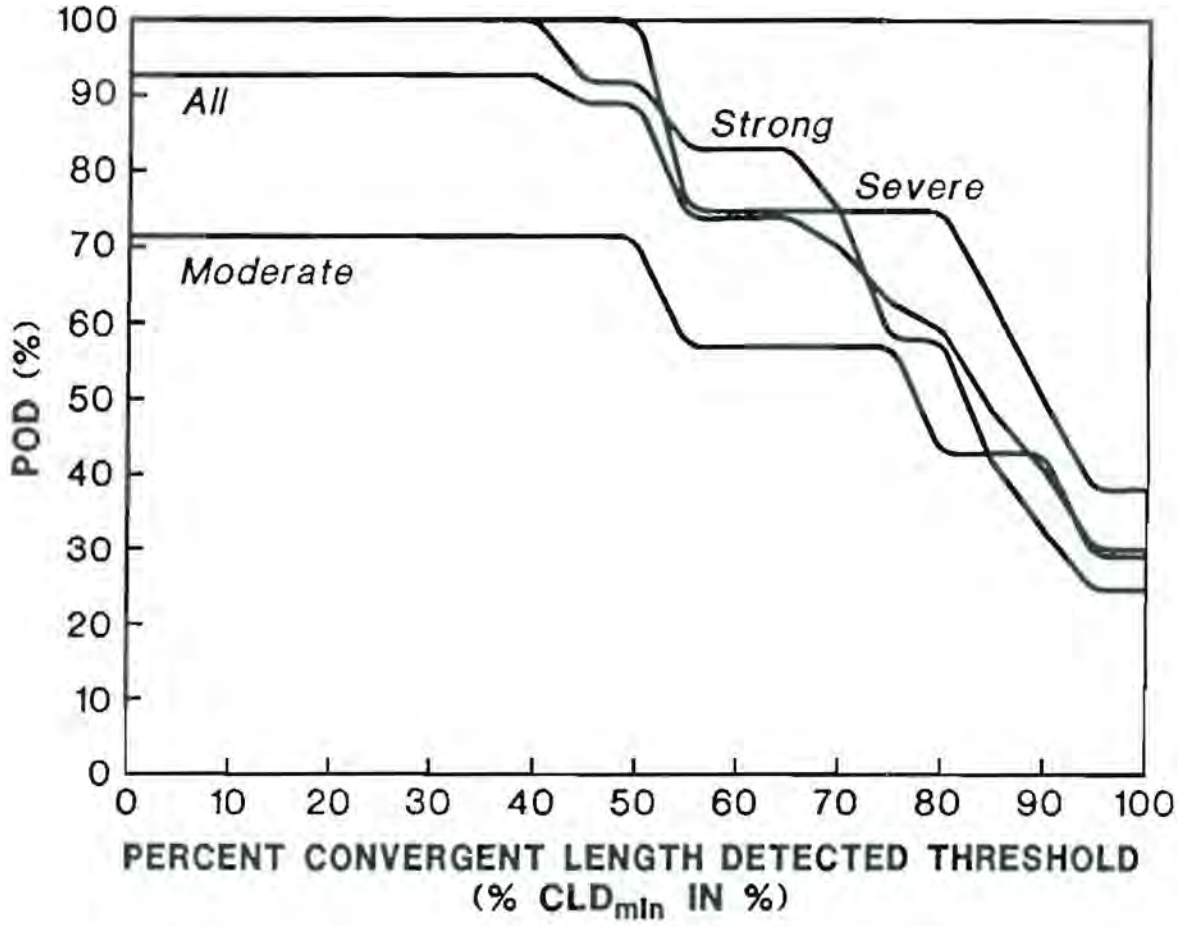

Figure 12. POD, as a function of Percent Convergent Length Detected Threshold (%CLD_{min}), for moderate, strong, severe and all gust fronts.

Table 3. POD and FAR statistics.

GUST FRONT ALGORITHM TEST RESULTS FROM DOPLIGHT 87 DATA

Date	Probability of Detection Moderate	Strong	Severe	Total true detections	False alarms	FAR(%)
3/16	1/1	4/4	2/2	7	0	0
5/21	4/6	6/6	2/2	17	0	0
5/24	-	2/2	4/4	6	1(6)	14(50)
Totals	5/7 71%	12/12 100%	8/8 100%	30	1(6)	3%(17%)

Table 4. Average Percent of Convergent Length Detected

GUST FRONT ALGORITHM TEST RESULTS FROM DOPLIGHT 87 DATA

Date	Average Percent of Convergent Length Detected Moderate	Strong	Severe	Total	Volume scans analyzed
3/16	90	93	100	95	6
5/21	81	68	75	74	8
5/24	-	78	76	77	6
Totals	83%	78%	82%	80%	20

9.B. FALSE ALARM RATIO (FAR)

An important measure of the confidence to be placed in the output of an algorithm is its False Alarm Ratio. If an algorithm has a high FAR, an observer may question the reliability of the algorithm's output, and possibly lose confidence in it. Thus, it

was decided that the Gust Front Algorithm must have a FAR of less than 10% to be considered a successful algorithm, regardless of how high the POD is. Therefore, for this phase of algorithm development, POD was sacrificed to maintain a low FAR.

As noted by Witt and Smith (1987), most false alarms occur when the environmental flow interacts with regions of ground clutter to produce spurious lines of radial convergence in the single Doppler velocity field. Thus, adequate suppression of ground clutter is essential so that the algorithm can maintain an acceptably low FAR.

1) COLORADO DATA

The FL-2 Doppler radar has an advanced ground clutter suppression system. It initially passes incoming data through a ground clutter filter (Evans, 1983) which removes most of the data contamination caused by ground clutter close to the radar. A residual clutter map is then used to suppress as much of the remaining clutter as possible (Mann, 1987). This is especially important for the Denver area, where the Front Range of the Rocky Mountains is within 60 km of the radar.

Table 1 shows the number of false alarms and the corresponding FAR for each of the eleven days analyzed. Most days had no false alarms, and the three days which did have false alarms, had FARs of 6% or less. Overall, the FAR was 3%.

2) OKLAHOMA DATA

The NSSL Doppler radar in Norman, unfortunately, does not have a ground clutter filter. Thus, suppression of false alarms was done through the use of clutter suppression windows. For the data analyzed, a circular window was used, centered on the radar, and extending out to 15 km.

Table 3 shows the number of false alarms and the corresponding FAR for each of the three days analyzed. We see that there was only one false alarm (on 24 May), resulting in an overall FAR of 3%. However, if the clutter suppression window had not been used, there still would not have been any false alarms on 16 March or 21 May, but on 24 May, six false alarms would have occurred. The overall FAR would then be 17%. This clearly illustrates the need for a sophisticated treatment of ground clutter suppression, as is done with the FL-2 radar.

9.C. PREDICTION EVALUATION

1) COLORADO DATA

Data from three days were used to determine the accuracy of the Gust Front Algorithm location forecasts. Two approaches were used, one that compares the forecasts to the actual true location at the forecast time, and another that estimates the timing accuracy of the location forecasts for gust fronts which passed through the mesonet.

The location scoring was done on a hit or miss basis, whereby a hit or miss is declared, based upon whether or not any

part of the forecast falls within ±2.5 km of the true location of the gust front. For example, a 10-minute forecast made at 21:00 is valid for 21:10 and this forecast is compared to the true location of the front at 21:10. If the forecast falls within ±2.5 km of the true location, a hit is declared. If it is outside ±2.5 km, a miss is declared. If the gust front dissipates (i.e., falls below a $\Delta V = 5$ m s^{-1} threshold) by 21:10, a false alarm is declared. POD and FAR statistics, as a function of gust front strength, for the 10- and 20-minute forecasts are shown in Table 5. As expected, the PODs increase as the gust front strength increases and are higher for the 10-minute forecast compared to the 20-minute forecast. Also, as expected, the FAR is higher for the 20-minute forecast compared to the 10-minute forecast, since there is a longer time period during which gust front dissipation can occur.

An attempt was also made to estimate how accurate the forecasts were in time. For instance, if a forecast showed that a gust front would arrive at the airport at 21:10 and the gust front actually arrived at 21:05, the forecast was 5 minutes late. Conversely, if the gust front was forecast to arrive at 21:10 and arrived at 21:15, the forecast was five minutes early. The time difference between forecast and truth was estimated from mesonet data and detections made at the forecast time.

Table 5. POD and FAR statistics for 10- and 20-minute forecasts.

GUST FRONT ALGORITHM TEST RESULTS FROM 1987 TDWR DATA

10-MINUTE FORECAST

Weak	Probability of Detection Moderate	Strong	All	False alarms	FAR(%)
11/19 58%	39/44 89%	20/21 95%	70/84 83%	7	8

20-MINUTE FORECAST

Weak	Probability of Detection Moderate	Strong	All	False alarms	FAR(%)
6/13 46%	20/37 54%	16/21 76%	42/71 59%	11	13

This analysis was performed on 24 10-minute forecasts and 20 20-minute forecasts. On the average, the 10- and 20-minute forecasts were about 2 and 1.5 minutes early, respectively. The standard deviation of the 10-minute forecast error was about 4.5 minutes, whereas the standard deviation of the 20-minute forecast error was roughly 6 minutes. Histograms of the time difference (in minutes) are shown in Figures 13 and 14.

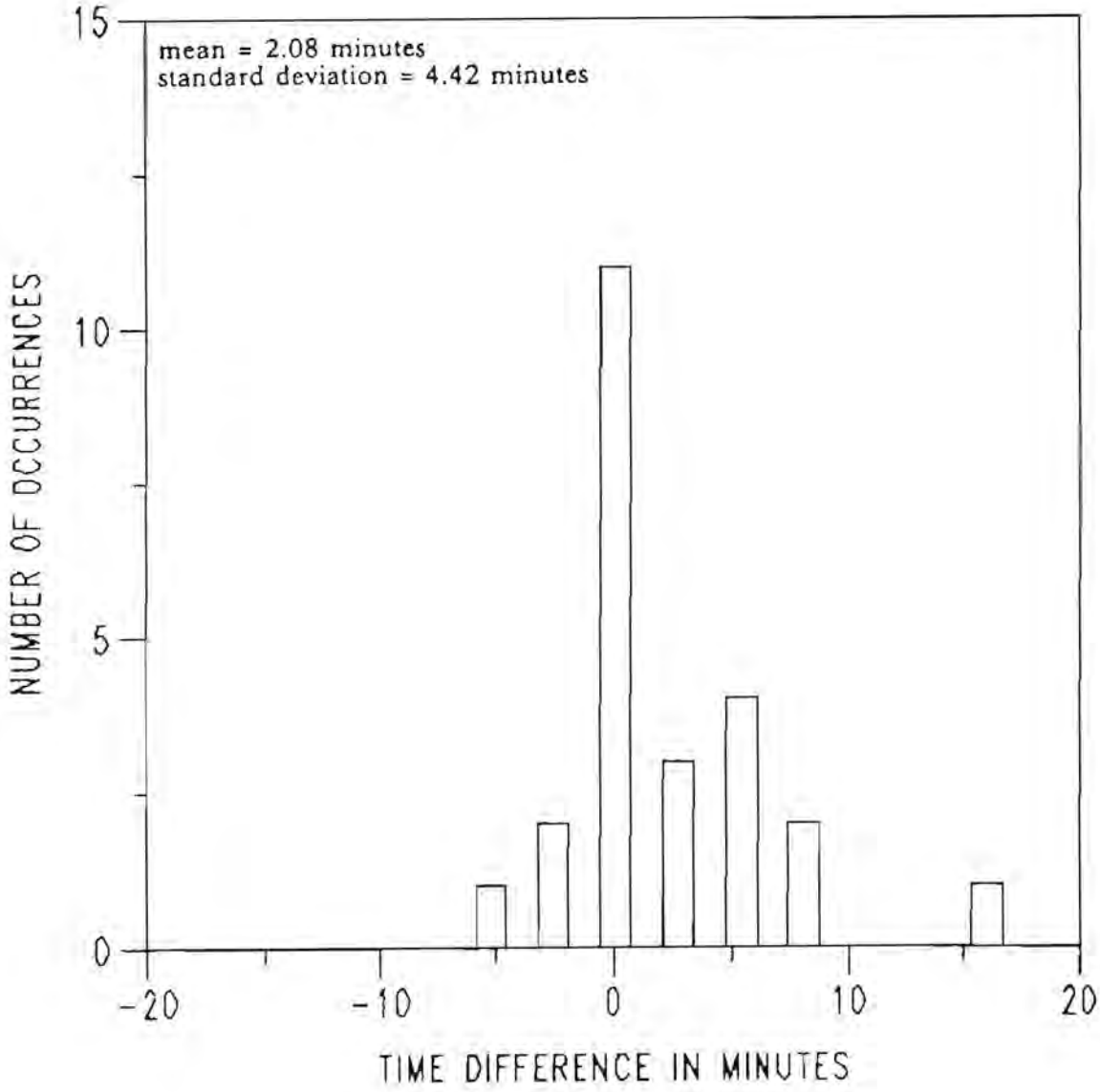

Figure 13. Histogram of time differences between 10-minute forecasts and actual positions. Negative (positive) values indicate a late (early) forecast.

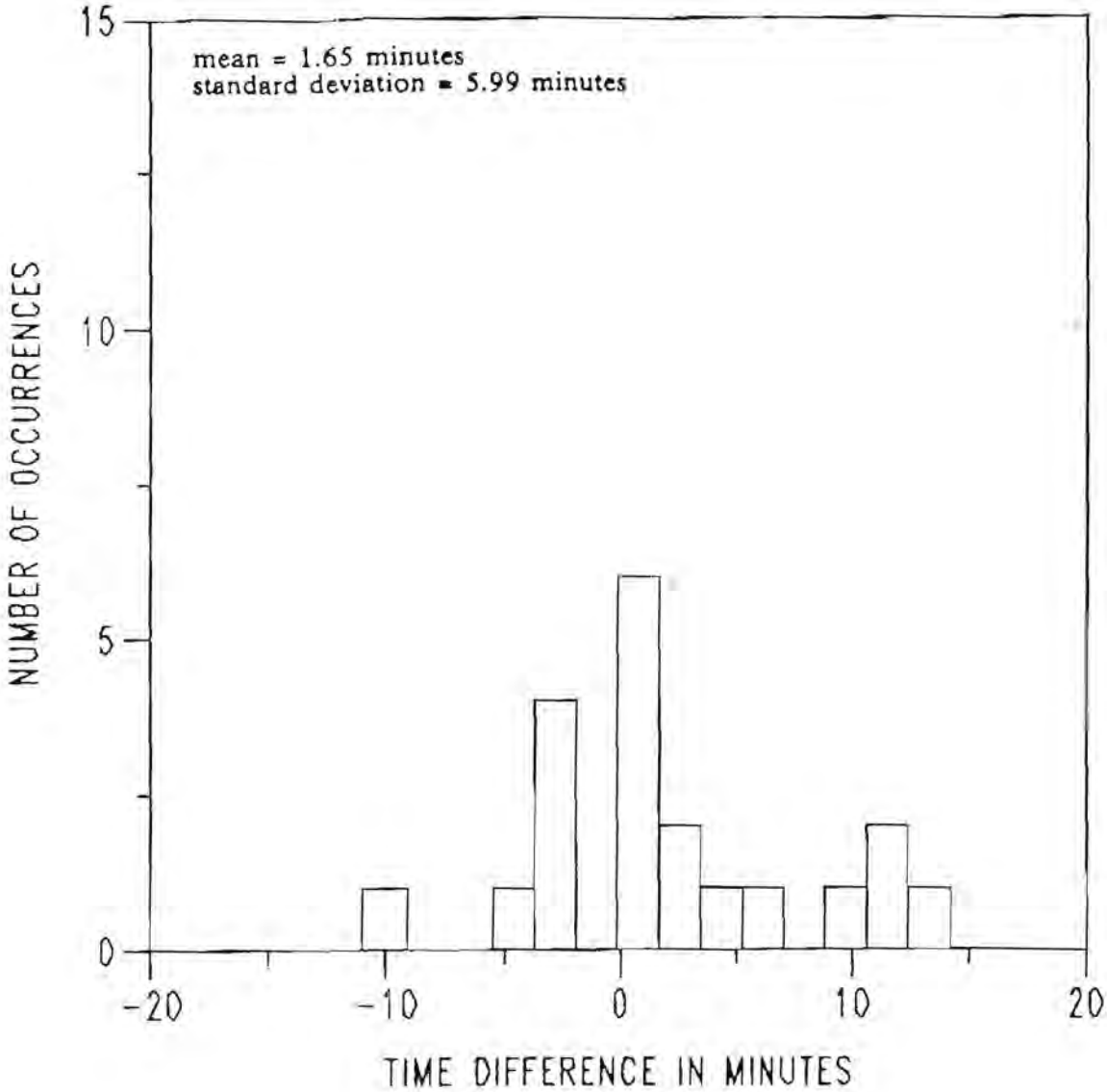

Figure 14. Histogram of time differences between 20-minute forecasts and actual positions. Negative (positive) values indicate a late (early) forecast.

Negative (positive) values are late (early) forecasts. Figures 15 and 16 show the distribution of the forecast time errors as a function of gust front strength. Timeliness of the forecasts (both 10- and 20-minute) tends to improve as gust front strength increases, as seen before. Also, the longer the detected length of a gust front, the better the forecast.

2) OKLAHOMA DATA

The accuracy of the algorithm location forecasts was determined by comparing the actual time of gust front passage over Will Rogers World Airport (OKC) to the predicted time of passage for one or more volume scans prior to the actual time of passage. Due to the fact that only one surface station was available for comparison, the analysis was more limited than for the Colorado data. The predicted time of passage was determined by taking the current location of a gust front and, using its propagation velocity, calculating the time it would pass over the airport if it maintained that velocity. Only forecasts less than 30 minutes ahead of the current time were used. The predicted time of passage was then compared to the actual time of passage. The results are shown in Table 6. Except for the 26-minute forecast made at 0004 CST on 25 May, all time differences between the actual frontal passage and predicted frontal passage are less than or equal to five minutes. The mean absolute error was 4.2 minutes. In general, magnitudes of time differences decreased as the lead time decreased.

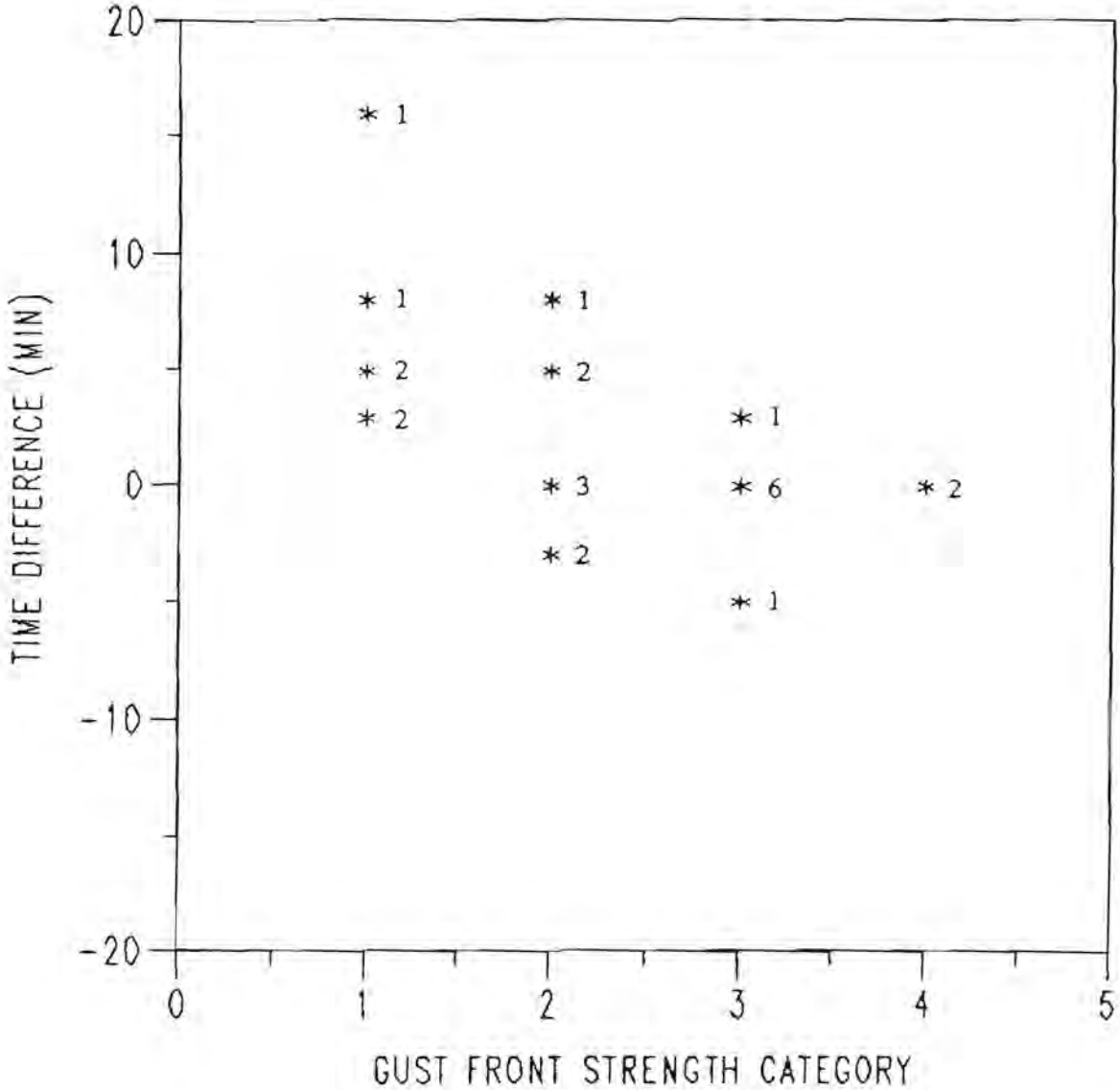

Figure 15. Time differences of 10-minute forecasts as a function of gust front strength. Category 1 gust fronts are weak, 2 are moderate, 3 are strong, and 4 are severe. The numbers beside the asterisks indicate the number of observations represented by the asterisk.

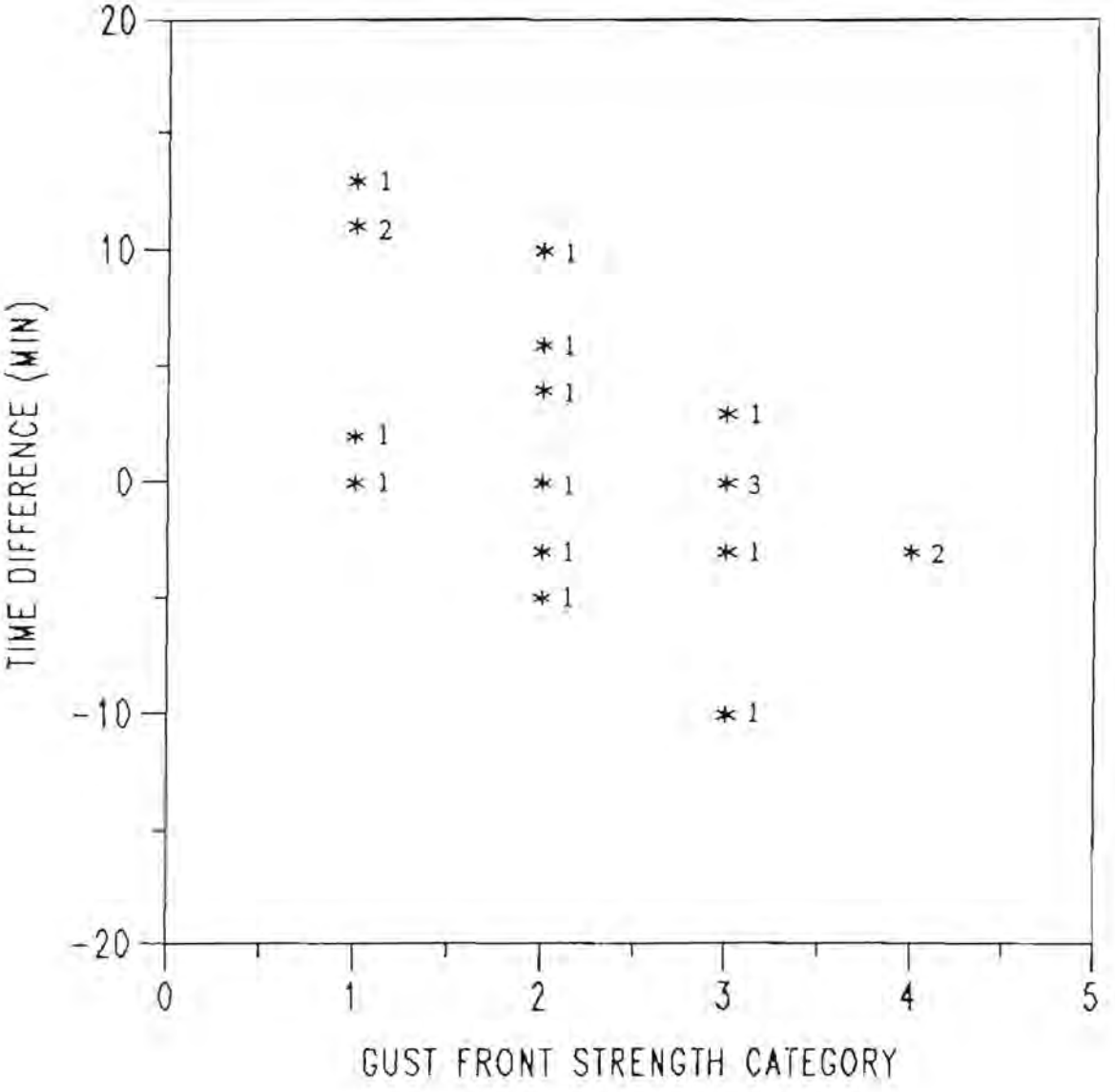

Figure 16. Time differences of 20-minute forecasts as a function of gust front strength. Category 1 gust fronts are weak, 2 are moderate, 3 are strong, and 4 are severe.

9.D. WIND ESTIMATE EVALUATION

The main objective of including the wind estimation technique in the Gust Front Algorithm is to provide a reliable estimate of the wind behind the detected gust front. For gust fronts located within the vicinities of Stapleton International Airport (Colorado Data) and Will Rogers World Airport (Oklahoma City), algorithm wind estimates behind the gust front are compared to surface observations.

Table 6. Comparison of the forecast time of frontal passage with the actual time of frontal passage.

GUST FRONT ALGORITHM TEST RESULTS FROM DOPLIGHT 87 DATA

Forecasts of the time of wind shift

Scan Time (CST)	Actual time of passage	Lead time (min)	Forecast time of passage	Time diff. (min)
		3/16/87		
2030	2053	23	2052	+ 1
		5/21/87		
2213	2230	17	2225	+ 5
2223		7	2232	- 2
		5/25/87		
0004	0030	26	0041	- 11
0011		19	0027	+ 3
0020		10	0027	+ 3

1) COLORADO DATA

The mesonet stations for algorithm ground truth for the Colorado data are located in close proximity to Stapleton International Airport and the height of the mesonet wind sensor is about 7 m. The LLWAS wind sensors are at slightly higher levels, but never exceed 25 m above ground. The locations of the mesonet stations, LLWAS sensors, Stapleton International Airport runways, and the FL-2 radar site are shown in Fig. 17. At a range of 15 km (roughly the range from FL-2 to Stapleton) and at an elevation angle of 0.5°, the center of the FL-2 radar beam is about 130 m above the ground. The radar and mesonets are not measuring winds at the same level of the atmosphere, thus discrepancies between the radar-measured and mesonet-measured winds due to vertical variations of the winds caused by surface friction are expected. However, since low level turbulent processes transport winds aloft to the ground, the peak winds measured at the surface mesonet stations provide a practical source of algorithm ground truth.

To determine which mesonet stations were behind a gust front, the location of the gust front from single Doppler radar data was superimposed on the plotted mesonet data. Data from those stations that had experienced a change in wind speed and/or wind direction were recorded and tabulated. For each mesonet station, the available wind data included the one-minute averages for speed and direction, and the peak speed of the one minute interval.

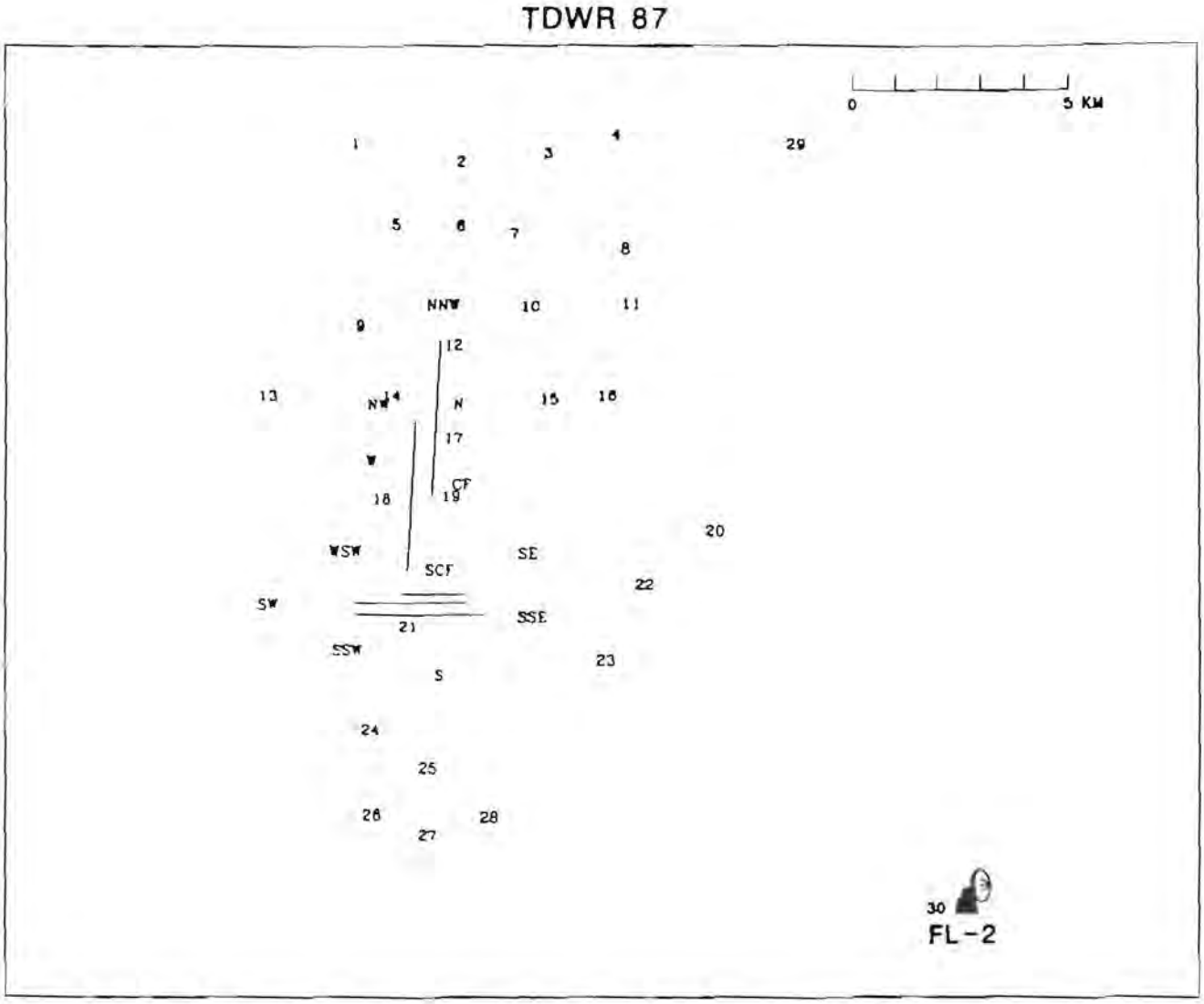

Figure 17. Location of mesonet stations, LLWAS sensors, Stapleton International Airport runways, and the FAA-Lincoln Laboratory FL-2 radar site.

To evaluate the algorithm-generated wind directions, a comparison between the average of the one-minute average directions over all mesonet stations behind the front and the algorithm estimate is made. A scatter plot of the

algorithm-generated wind directions and the average of the one-minute average direction is shown in Fig. 18. In general, the agreement between the algorithm directions and the mesonet data is quite good, with only a small amount of scatter about a one-to-one correspondence line.

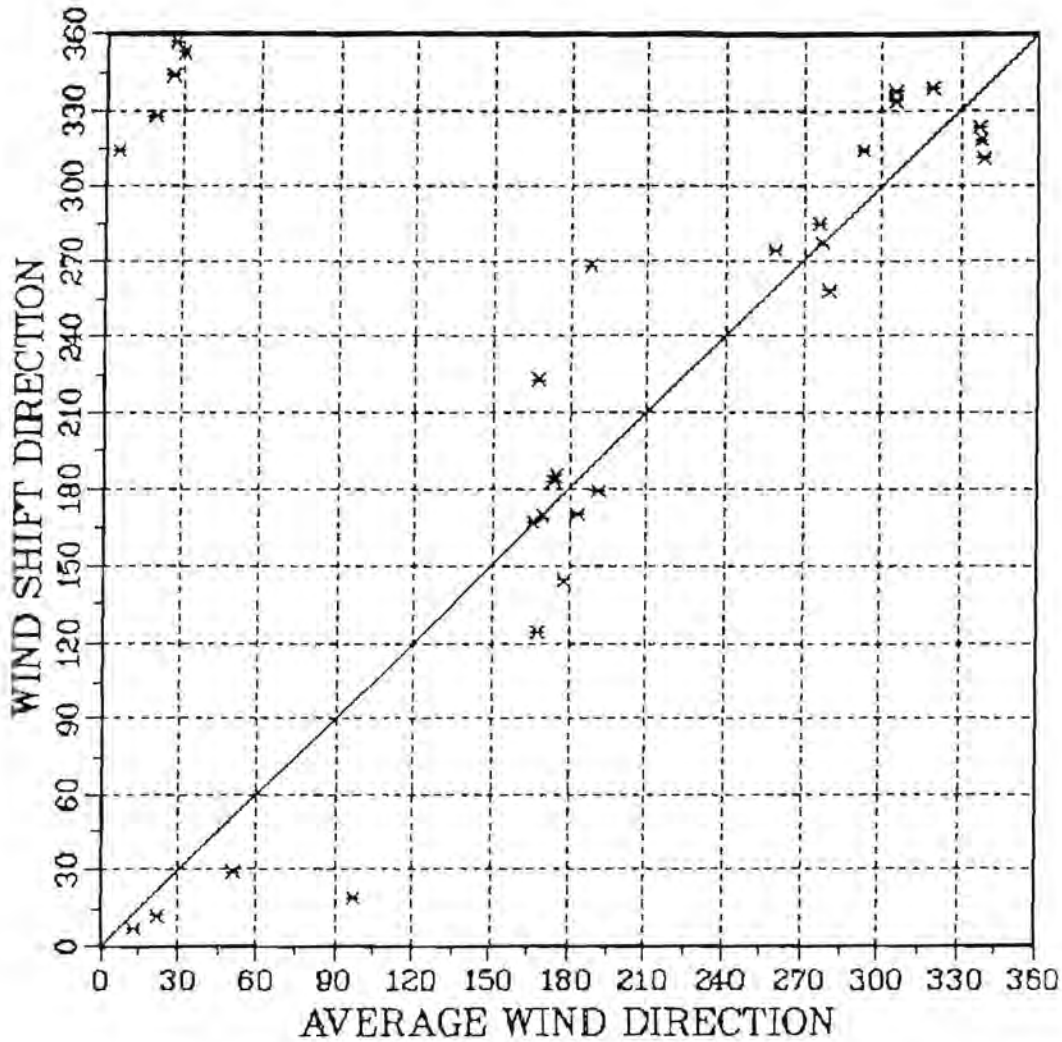

Figure 18. Scatter plot of wind direction computed by the wind shift algorithm versus the average wind direction computed from mesonet data. The solid line represents a one-to-one correlation between the variables.

Figure 19 is a plot of the differences (mesonet - algorithm) in wind direction. The average absolute difference is equal to 25°, with a standard deviation of 37°. In general, the differences between mesonet and algorithm wind directions are positive values, indicating that the algorithm directions had a tendency to be somewhat cyclonic (counterclockwise) of the mesonet-derived directions. There is a paucity of data for average wind directions between both the 210°-245° interval, as well as the 30°-65° interval, since the flow for these directions is perpendicular to the radar beam as it sweeps across the mesonet. Under such conditions, gust fronts are not detected by the algorithm and therefore, a wind estimate is not computed.

The wind speeds computed by the algorithm are compared to the averaged (over selected stations) one-minute average speeds, the averaged peak speeds, and the overall peak speeds. Of these, the algorithm correlates best with the average peak speed (Fig. 20). The average absolute difference between the algorithm generated and the averaged peak speed is equal to 2.5 m s^{-1}, with a standard deviation of 1.6 m s^{-1}. Because wind speed generally increases with height and higher momentum air is transported to the ground by turbulent eddies, it is not surprising that the algorithm estimated wind speeds are most directly related to the average peak speed measured by the mesonet sensors behind the front.

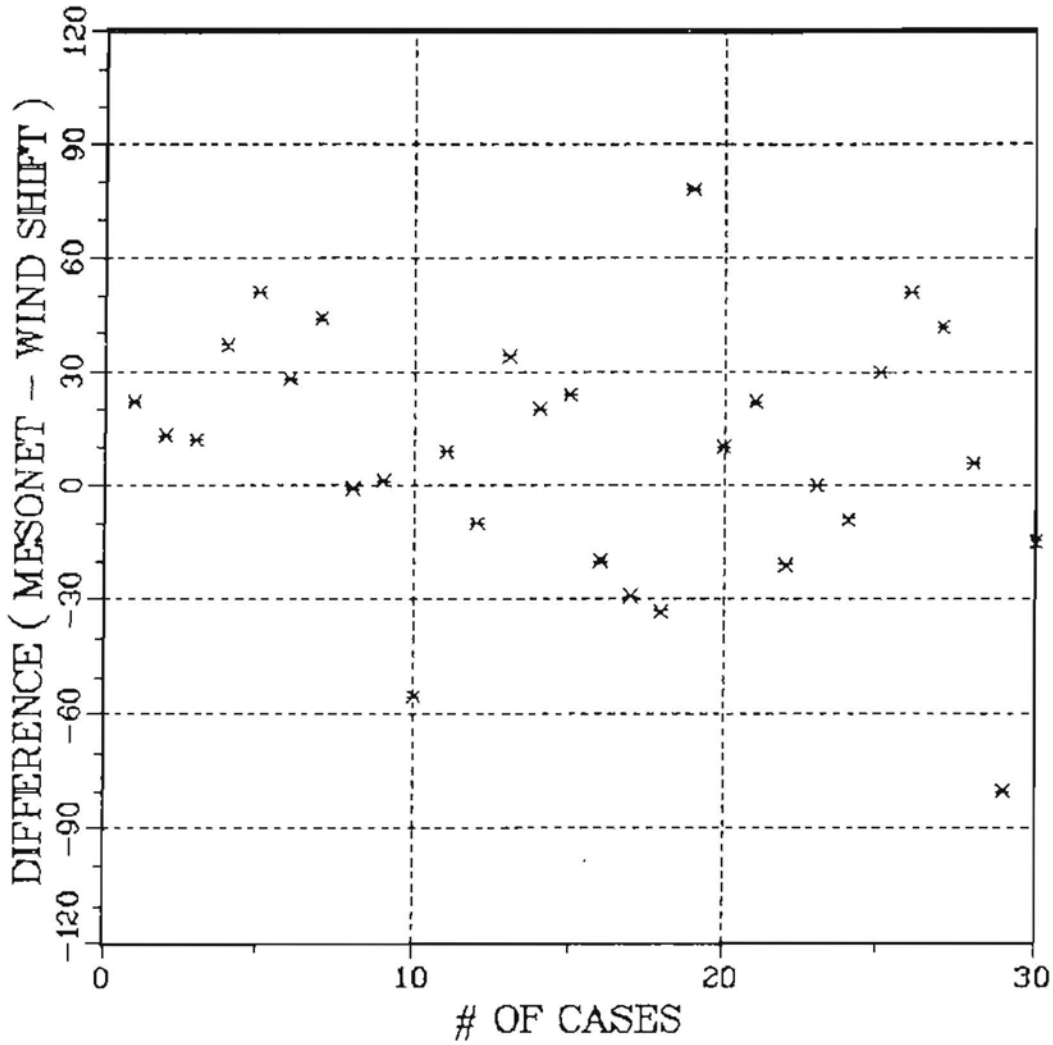

Figure 19. Difference between algorithm direction estimates and average wind directions computed from mesonet data.

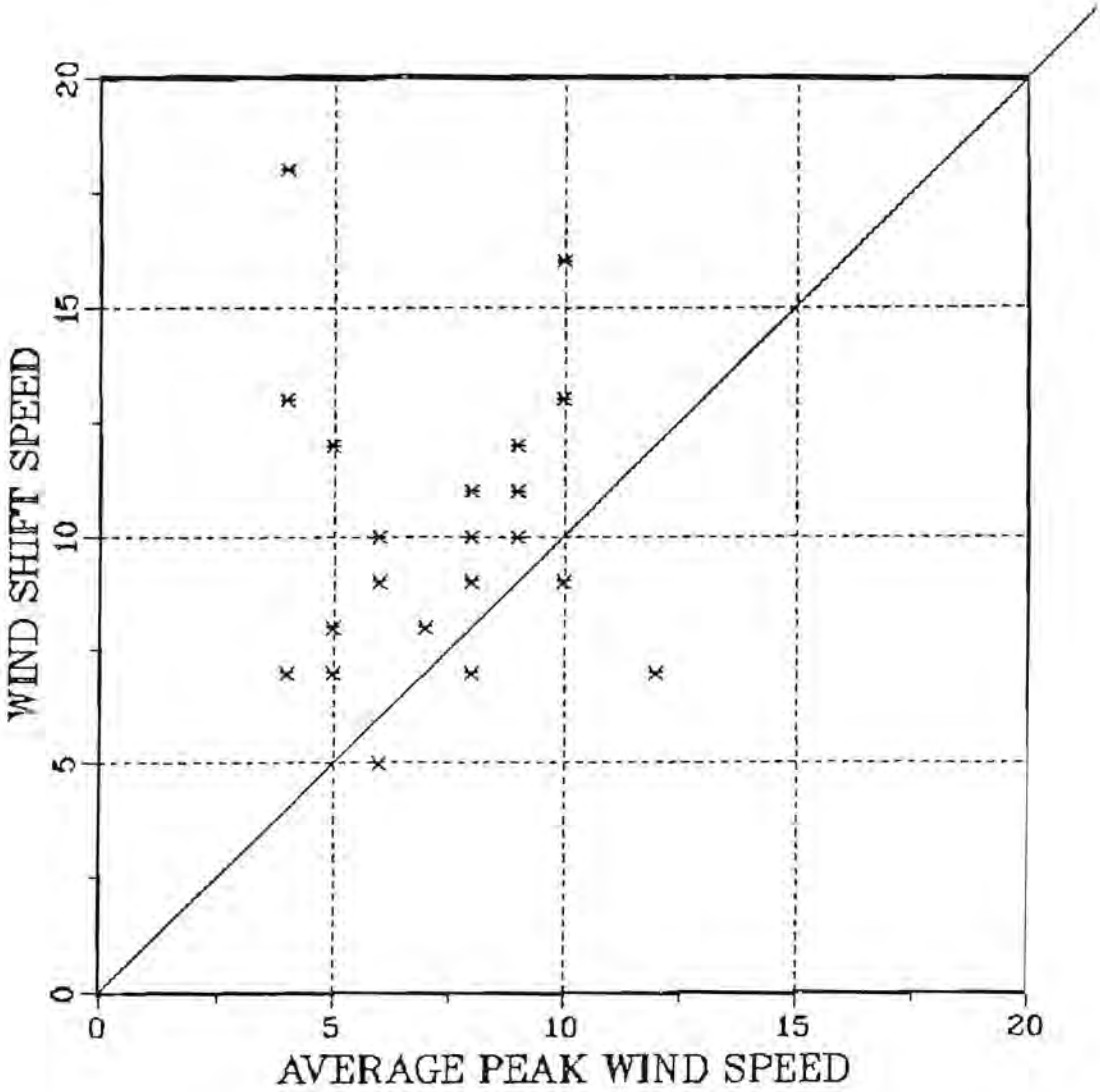

Figure 20. Scatter plot of wind speeds computed by wind shift algorithm versus averaged peak wind speed from mesonet data. The solid line represents a perfect correlation between the variables.

2) OKLAHOMA DATA

The algorithm's wind shift estimates obtained from the Oklahoma data were evaluated in a slightly different manner than the Colorado data. This is again due to the fact that we are

using only one surface station for the analysis. For the Oklahoma data, algorithm wind estimates from times prior to frontal passage at Oklahoma City are compared with surface wind observations at Oklahoma City, after frontal passage. Surface winds and algorithm estimates are shown in Table 7, along with the lead time of the algorithm estimates.

As noted in the previous section, algorithm wind speeds compare best with peak surface speeds (wind gusts). For the Oklahoma data, the mean absolute difference between algorithm wind speeds and peak surface speeds was 2.6 m s^{-1}. The mean absolute differences between algorithm direction estimates and actual directions was 33°. These differences are slightly larger than those computed from the Colorado data. A portion of the differences, however, can be attributed to the small sample size (six cases) and time difference (lead time) between the algorithm estimates and the surface wind observations.

Table 7. Comparison of algorithm wind estimates with actual wind observations. (U) indicates uniform wind model, (P) indicates perpendicular wind model.

GUST FRONT ALGORITHM TEST RESULTS FROM DOPLIGHT 87 DATA

Wind Shift Algorithm Evaluation

Scan time (CST)	Lead time (min)	Wind observed after passage (kts)	Wind estimate after passage (kts)
		3/16/87	
2030	23	280/17G30	252/24 (U)
		5/21/87	
2213	17	300/10G16	302/15 (P)
2223	7		323/13 (U)
		5/25/87	
0004	26	330/19G25	303/28 (U)
0011	18		257/23 (U)
0020	9		289/10 (P)

3) MODEL COMPARISON

As part of the evaluation of the wind shift portion of the Gust Front Algorithm, a comparative study of the two models used to produce the horizontal wind estimates behind the gust front was completed. Using the Colorado data, two wind estimates for each gust front are computed by, (a) assuming a uniform, horizontal wind (uniform wind model) within the processing sector, and (b) assuming a horizontal wind perpendicular to the

gust front orientation (perpendicular wind model) within the processing sector.

Using the average (stations behind the front) of the one-minute average mesonet directions, the algorithm-generated directions from the two models are evaluated. Average absolute difference between mesonet and uniform wind estimates is equal to 27°, with a standard deviation of 40°. The absolute difference between mesonet and perpendicular wind estimates is equal to 31°, with a standard deviation of 37°.

Algorithm-generated wind speed estimates from the two models are also evaluated, with comparisons made against the averaged (stations behind the front) one-minute average speed, average peak speed, and overall peak speed. The best comparison of algorithm-generated speeds is with the average peak speeds from the selected mesonets. Speed comparison results are summarized in Table 8.

This study shows that the uniform wind estimates are reasonable estimates of winds behind the gust fronts, and also shows that in general, uniform wind estimates are slightly better than just assuming that the winds are perpendicular to the gust front. However, when uniform estimates are rejected by algorithm error checking, the perpendicular wind model provides a valid replacement estimate.

Table 8. Comparison of algorithm-generated and mesonet wind speeds.

	Absolute Difference ($m\ s^{-1}$)	
	Uniform Wind	Perpendicular Wind
One-Minute Average	3.7	3.2
Average Peak	2.6	2.3
Overall Peak	4.5	4.6

	Standard Deviation ($m\ s^{-1}$)	
	Uniform Wind	Perpendicular Wind
One-Minute Average	2.2	2.3
Average Peak	1.6	2.0
Overall Peak	2.5	3.3

10. SUMMARY AND CONCLUSIONS

Over the past two years work has continued on Gust Front Algorithm development and testing. In addition to improvements in the preprocessing of radar data (ground clutter suppression and reliable velocity dealiasing), numerous enhancements to the algorithm have been made. Algorithm detection and tracking performance has benefited by inclusion of 1) peak velocity difference thresholding, 2) variable thresholds for the two elevation scans, 3) connection of nearby shear features (convergence lines) into a single shear feature, 4) a fifth-order polynomial fit to the radial convergence lines to allow more representative positioning of the gust front, and 5) normal velocity component tracking and forecasting. Improvements in the wind estimation technique include: 1) a velocity data outlier rejection scheme, 2) redefinition of the data processing sector,

3) a perpendicular wind estimation technique for use with short gust fronts and as a replacement estimate when uniform wind model estimates fail error checks, and 4) rigorous error checking of wind estimates using gust front orientation and tracking information.

The performance evaluation of the current version of the algorithm was completed using the 1987 Colorado and Oklahoma data sets. The most notable results, related to the algorithm improvements, are the high probability of detecting any part of a gust front and the low FARs.

For the selected Colorado cases, greater than 90% of all strong and severe gust fronts were detected, while 79% of all gust fronts classified as moderate were also detected. The algorithm achieved a FAR of $\leq$ 3%. Analysis of algorithm wind estimates behind gust fronts passing over the airport showed that 67% of the wind direction estimates were within 30° of ground truth wind directions. Wind speed estimates were an average of 2.5 m s^{-1} different than average peak speeds from mesonet ground truth. The algorithm's 10- and 20-minute forecasted locations were on the average 1.5-2.0 minutes early. However, as gust front strength increased, the algorithm's prediction capability improved.

Results from the Oklahoma data were generally similar to results from the Colorado data. Again, greater than 90% of all strong and severe gust fronts were partially detected, with 71% of moderate gust fronts partially detected. There was only one

false alarm, giving a FAR of 3%. All but one of the forecasts of the time of frontal passage over the airport were within five minutes of the actual observed time of passage. The mean absolute error was 4.2 minutes. Analysis of algorithm wind estimates, behind gust fronts passing over the airport, showed that the mean absolute difference between algorithm wind speeds and peak surface wind speeds was 2.6 m s^{-1}. The mean absolute difference between algorithm direction estimates and actual directions was 33°.

Further improvements to the algorithm may allow for a higher percentage of total gust front length to be detected. Additional pattern recognition techniques could be implemented after the radial convergent part of a gust front is detected. Inclusion of techniques to detect reflectivity thin lines and azimuthal shear, along with lowering radial convergence thresholds at gust front edges, should help increase the length of detected fronts. Intermittent detections of gust fronts have also been an occasional problem. Time consistency of gust front detections may be enhanced by maintaining gust front detections and wind shift information for one scan at the five minute predicted location for missed detections.

Although several improvements to the Gust Front Algorithm are planned, in its present form, the algorithm has successfully exploited its ability to detect patterns of radial convergence from Doppler radar velocities. With the latest enhancements to the algorithm, in addition to the five years of testing and

development, an effective operational tool to be used by Air Traffic Control is nearing reality with the inclusion of this version of the Gust Front/Wind Shift Algorithm in TDWR.

11. REFERENCES

Donaldson, R.J., R.M. Dyer, and M.J. Kraus, 1975: "An objective evaluator of techniques for predicting severe weather events", 9th Conference on Severe Local Storms, Norman, Oklahoma, Amer. Meteor. Soc., Boston, MA, 321-326.

Eilts, M.D., and S.D. Smith, 1989: "Efficient Doppler velocity dealiasing using local environmental constraints", accepted by J. Atmos. Oceanic Tech.

Evans, J.E., 1983: "Ground clutter cancellation for the NEXRAD system", MIT/Lincoln Laboratory Report. ATC-122, 182 pp.

Forsyth, D.E., D.W. Burgess, L.E. Mooney, M.H. Jain, C.A. Doswell III, W.D. Rust, and R.M. Rabin, 1989: "Doplight '87 Program Summary". NOAA Tech. Memo, in press.

Klingle-Wilson, D.L., S.H. Olson, W. Wilson, W.P. Mahoney, III, S.D. Smith, A. Witt, and M.D. Eilts, 1989: "Gust front detection algorithm for the Terminal Doppler Weather Radar: Part II, Performance assessment", 3rd International Conference on the Aviation Weather System, Anaheim, CA, Amer. Meteor. Soc., Boston, MA, 398-402

Mann, D.R., 1988: "TDWR clutter residue map generation and usage", FAA Report No. DOT/FAA/PM-87-26 (ATC-148), 34 pp.

McCarthy, J., J.W. Wilson, and M.R. Hjelmfelt, 1986: "Operational wind shear detection and warning: The "CLAWS" experience at Denver and future objectives", Preprints, 23rd Conference on Radar Meteorology, Snowmass, Colorado, Amer. Meteor. Soc., Boston, MA.

Smith, S.D., 1986: "Sectorized uniform wind algorithms", NEXRAD Joint Systems Program Office Report, Sept. 1986. 25 pp.

Smith, S.D., and R.M. Rabin, 1989: "Considerations in estimating horizontal wind gradients from an individual Doppler radar or a network of wind profilers", J. Atmos. Oceanic Tech., 6, 446-458.

Uyeda, H. and D.S. Zrnić, 1985: "Automatic detection of gust fronts", FAA Report No. DOT/FAA/PM-85/11.

Uyeda, H. and D.S. Zrnić, 1986: "Automatic detection of gust fronts", J. Atmos. Oceanic Tech., 3, 36-50.

Witt, A., and S.D. Smith, 1987: "Development and testing of the gust front algorithm", FAA Report No. DOT/FAA/PS-87/4.

APPENDIX A

GUST FRONT/WIND SHIFT DETECTION ALGORITHM OUTLINE

I. FOR EACH TILT

1) For each radial

   a) Edit Doppler velocities based on

      1) reflectivity threshold

      2) signal-to-noise threshold

   b) Dealias velocities

   c) Smooth velocities (does not reduce data density)

      1) if gate spacing < 200 m, 9 gate running average

      2) if gate spacing ≥ 200 m, 7 gate running average

   d) Locate shear segments

      1) find runs of decreasing velocity in range

      2) calculate peak shear over 8 gates (6 if gate spacing ≥200 m)

      3) threshold shear segments

         a) velocity difference between end points of segments

            1) 7 m s^{-1} for 0.5° elevation angle

            2) 5 m s^{-1} for 1.0° elevation angle

         b) peak shear (2×10^{-3} s^{-1})

         c) if peak velocity difference is greater than velocity difference, discard

4) consolidate important attributes of valid shear segments into pattern vectors

a) azimuth

b) range to peak shear

c) peak shear

d) velocity difference between end points

2) Build Features

a) two pattern vectors are associated if they are within

1) azimuth threshold (2.2°)

2) range threshold (2.0 km)

b) if number of vectors in feature < 5, disregard

c) if end point to end point feature length < 5 km, disregard

3) Feature Connection

if end points defined by locations of peak shear of two features are within 5 km, the features are merged

II. FOR EACH VOLUME SCAN

1) Check Vertical Continuity

a) rectangular vertical search

b) select largest feature in rectangle to represent the front

c) if end point to end point length of largest feature < 10 km, discard

2) Special Case Features to Add

   a) largest feature if length ≥ 15 km

   b) feature at upper tilt if length ≥ 10 km and range ≤ 10 km

3) Polynomial Curve Fitting

   a) calculate path length of merged features

   b) fit valid feature with high-order polynomial, using vector locations from both low-level tilts

      1) third-order polynomial if length ≤ 20 km

      2) fifth-order polynomial if length > 20 km

   c) plot fitted curve

4) Windshift Calculation

   a) define data processing sectors, one on each side of the gust front

      1) azimuthal width of sector equals azimuthal extent of gust front

      2) range width of sector is 30 gates (about 4 km)

      3) displace sectors 2 km from detected gust front

   b) select model based on azimuthal extent of gust front

      1) a) assume uniform, horizontal wind if azimuthal extent is ≥ 30°

         b) compute horizontal wind perpendicular to gust front orientation; is replacement

estimate when uniform, horizontal wind estimate fails error checks

2) assume horizontal wind perpendicular to gust front orientation if azimuthal extent < 30°

c) fit radar velocity data to selected model using two-pass least-squares fit

1) reject data which deviate by more than two root mean squared errors from least-squares fitted values

2) refit edited radar data to selected model

d) determine from tracking information which processing sector is on the outflow side (i.e., behind the front)

1) replace uniform, horizontal winds that are quasi-parallel to gust front orientation with horizontal wind estimates perpendicular to the front

2) reject any wind estimates behind the front if wind direction has a component opposite to front propagation direction

3) set perpendicular wind estimates ahead of front to missing value

5) Check Time Continuity

a) calculate distances separating gust front centroids at consecutive radar scans

1) time continuity established if distance between two centroids less is than the product of 33 m s^{-1} and the time separation between volume scans

2) plot wind estimate behind the gust fronts which have time continuity

b) forecast future position of gust front

1) calculate component of motion perpendicular to gust front orientation from centroid displacement

2) project gust front to future positions (5, 10, or 20 min forecast)

APPENDIX B

SITE-ADAPTABLE PARAMETERS FOR THE GUST FRONT DETECTION ALGORITHM

Parameter	Suggested Value	Sensible Range
VELOCITY DIFFERENCE		
LOWER TILT	7.0 m s^{-1}	5.0 - 10.0 m s^{-1}
UPPER TILT	5.0 m s^{-1}	4.0 - 8.0 m s^{-1}
PEAK SHEAR		
LOWER TILT	2.0 m s^{-1} km^{-1}	2.0 - 4.0 m s^{-1} km^{-1}
UPPER TILT	2.0 m s^{-1} km^{-1}	2.0 - 4.0 m s^{-1} km^{-1}
AZIMUTH OVERLAP	2.2°	2.0° - 4.0°
RANGE OVERLAP	2.0 km	2.0 - 3.0 km
NUMBER OF SEGMENTS	5	5 - 10
FEATURE LENGTH	5.0 km	3.0 - 10.0 km
FEATURE DISTANCE	5.0 km	3.0 - 6.0 km
COMBINED LENGTH	5.0 km	5.0 - 10.0 km
FRONT LENGTH	10.0 km	10.0 - 20.0 km
AUTO PLOT LENGTH	15.0 km	10.0 - 20.0 km

VELOCITY DIFFERENCE = Threshold value(s) for velocity difference across a potential shear segment for it to be identified as a valid shear segment. There are separate thresholds for each radar tilt.

PEAK SHEAR = Threshold value(s) for peak shear for a shear segment to be identified as a valid shear segment. There are separate thresholds for each tilt.

AZIMUTH OVERLAP = Maximum angular spacing allowed to associate two shear segments.